Top Curr Chem (2016) 368: 61–96
DOI: 10.1007/128_2014_611

Published online: 20 March 2015

Constricted Variational Density Functional Theory Approach to the Description of Excited States

Tom Ziegler, Mykhaylo Krykunov, Issaka Seidu, and Young Choon Park

Abstract We review the theoretical foundation of constricted variational density functional theory and illustrate its scope through applications.

Keywords Constricted variational density functional theory • Density functional theory • Time-dependent density functional theory

Contents

1 Introduction

Excited states have been studied in wave function theory by both excited state variational theories and ground state response methods [1, 2]. Either approach has been used extensively and is considered complementary and, in principle, able to

T. Ziegler (✉), M. Krykunov, I. Seidu, and Y.C. Park
Department of Chemistry, University of Calgary, Calgary, AB, Canada T2N1N4
e-mail: ziegler@ucalgary.ca

afford estimates to any desired degree of accuracy. Given the status of Kohn–Sham density functional theory (KS-DFT) as a ground state theory, the natural path to excited states in KS-DFT would seem to be the ground state response approach. In fact, Runge and Gross [3] have formulated a time-dependent density functional ground state response theory (TDDFT) which in principle should be able to describe excited state properties without approximations. TDDFT in its exact form requires knowledge of the "true" ground state functional and of the frequency dependence of the energy response kernel corresponding to this functional. In practical calculations, use is made of approximate ground state functionals and the frequency dependence of the kernel is neglected in what has now become known as the adiabatic TDDFT approach (ATDDFT) [4–9]. For more than two decades the ATDDFT approach has remained the method of choice in DFT-based studies of excited states and both its merits and limitations have been studied in great detail [10–33]. Progress beyond the adiabatic approximation has, on the other hand, been slow, although work in this direction is ongoing [34–36].

Long before TDDFT, Slater introduced a variational DFT approach to excited states called ΔSCF [37, 38]. Excited states are reached in this scheme by promoting electrons from occupied to virtual ground state levels followed by a KS calculation on the new electron configuration. The ΔSCF approach has met with considerable success for those lower excited states which can be represented by a single orbital replacement (SOR) [39–49]. However, it is plagued by SCF-convergence problems. Further, as it applies a ground state functional in a variational excited state calculation, it is considered somewhat ad hoc [50] and without any theoretical foundation [51–53]. Nevertheless, Van Voorhis et al. [39] have recently put forward some theoretical justifications for ΔSCF and Besley et al. [42, 43] and Park et al. [44] have addressed the SCF-convergence issue. Apart from ΔSCF, there are a number of interesting variational DFT approaches to the study of excited states. They include ensemble DFT [54–59], variation of bifunctionals [60], and excited state perturbation theory [61]. They are discussed elsewhere in this volume.

The use of a ground state functional in variational excited state calculations seems intuitively appealing from the point of view that electron correlation should be quite similar in the ground and excited states, at least in the lower valence region. In fact, based on this notion we introduced in 2009 the constricted variational DFT method (CV-DFT) for excited states [29]. In this theory we allow for an admixture of virtual ground state orbitals $\{\psi_a; a = 1, \mathrm{vir}\}$ into each of the occupied ground state orbitals $\{\psi_j; j = 1, \mathrm{occ}\}$, according to

$$\psi_i = \sum_a^{\mathrm{vir}} U_{ai}\psi_a \tag{1}$$

The ansatz in (1) makes it possible to construct occupied excited state orbitals and evaluate the corresponding excited state energies based on the ground state functional to any desired order n in the variational mixing matrix $\mathbf{U}$. Such a

procedure gives rise to the *n*th order CV-DFT scheme designated as CV(*n*)-DFT [26–28].

We start this review by an outline of the CV(*n*)-DFT theory. This framework enables us to identify ATDDFT and ΔSCF as special cases of the CV(*n*)-DFT scheme with ATDDFT being equivalent to CV(2)-DFT [29, 62] whereas ΔSCF corresponds to CV(∞)-DFT under the simplifying assumption that the excited state under investigation can be described by a single orbital replacement $(i \rightarrow a)$ [27, 44]. The theoretical exposition is followed by first assessing the general performance of CV(*n*)-DFT in connection with applications to $n \rightarrow \pi^*$ [26–67] and $\pi \rightarrow \pi^*$ [27] transitions in organic molecules. After that we demonstrate that CV(*n*)-DFT is able to deal with a number of transitions where the performance of ATDDFT based on local and hybrid functionals is problematic. These transitions involve $\pi \rightarrow \pi^*$ excitations in organic dyes [64, 65] as well as $\pi \rightarrow \pi^*$ transitions in charge transfer adducts [30] and Rydberg excitations for atoms and small molecules [66]. We finally discuss future directions for the development and application of the CV(*n*)-DFT scheme.

2 Constricted Variational Density Functional Theory

We have recently introduced a variational approach based on density functional theory for the description of excited states [29, 31]. In this constricted variational density functional theory, CV-DFT, we carry out a unitary transformation among occupied $\{\phi_i; i = 1, \mathrm{occ}\}$ and virtual $\{\phi_a; a = 1, \mathrm{vir}\}$ ground state orbitals:

$$Y\begin{pmatrix}\phi_{\mathrm{occ}}\\ \phi_{\mathrm{vir}}\end{pmatrix} = \mathrm{e}^{\mathbf{U}}\begin{pmatrix}\phi_{\mathrm{occ}}\\ \phi_{\mathrm{vir}}\end{pmatrix} = \left(\sum_{m=0}^{\infty}\frac{(\mathbf{U})^m}{m!}\right)\begin{pmatrix}\phi_{\mathrm{occ}}\\ \phi_{\mathrm{vir}}\end{pmatrix} = \begin{pmatrix}\phi'_{\mathrm{occ}}\\ \phi'_{\mathrm{vir}}\end{pmatrix} \tag{2a}$$

Here ϕ_{occ} and ϕ_{vir} are concatenated column vectors containing the sets $\{\phi_i; i = 1, \mathrm{occ}\}$ and $\{\phi_a; a = 1, \mathrm{vir}\}$ whereas ϕ'_{occ} and ϕ'_{vir} are concatenated column vectors containing the resulting sets $\{\phi'_i; i = 1, \mathrm{occ}\}$ and $\{\phi'_a; a = 1, \mathrm{vir}\}$ of occupied and virtual excited state orbitals, respectively. The unitary transformation matrix Y in (2a) is expressed in terms of a skew symmetric matrix $\mathbf{U}$ as

$$Y = \mathrm{e}^{\mathbf{U}} = \mathbf{I} + \mathbf{U} + \frac{\mathbf{U}^2}{2} + \cdots = \sum_{m=0}^{\infty}\frac{\mathbf{U}^m}{m!} = \sum_{m=0}^{\infty}\frac{\left(\mathbf{U}^2\right)^m}{2m!} + \mathbf{U}\sum_{m=0}^{\infty}\frac{\left(\mathbf{U}^2\right)^m}{(2m+1)!} \tag{2b}$$

If the summation in (2a) and (2b) over m is carried out to $m = n$ we talk about *n*th order CV-DFT or CV(*n*)-DFT. Above $U_{ij} = U_{ab} = 0$ where "*i*,*j*" refer to the occupied set $\{\phi_i; i = 1, \mathrm{occ}\}$ whereas "*a*,*b*" refer to $\{\phi_a; a = 1, \mathrm{vir}\}$. Further, U_{ai} are the variational mixing matrix elements of (1) which combines virtual and occupied ground state orbitals in the excited state with $U_{ai} = -U_{ia}$. Thus the entire

matrix **U** is made up of occ × vir independent elements U_{ai} which can also be organized in the column vector $\vec{U}$. For a given $\vec{U}$ we can, by means of (2a) and (2b), generate a set of "occupied" excited state orbitals:

$$\phi_i^{'} = \sum_{p}^{\text{occ+vir}} Y_{pi}\phi_p = \sum_{j}^{\text{occ}} Y_{ji}\phi_j + \sum_{a}^{\text{vir}} Y_{ai}\phi_a \tag{3}$$

which are orthonormal to any order in U_{ai}.

2.1 Second Order Constricted Variational Density Functional Theory

In the simple CV(2)-DFT theory [29] the unitary transformation of (2a) and (2b) is carried out to second order in **U**. We thus obtain the occupied excited state orbitals to second order as

$$\phi_i^{'} = \phi_i + \sum_{a}^{\text{vir}} U_{ai}\phi_a - \frac{1}{2}\sum_{j}^{\text{occ}}\sum_{a}^{\text{vir}} U_{ai}U_{aj} \tag{4}$$

from which we can generate the excited state Kohn–Sham density matrix to second order as

$$\begin{aligned}\rho'(1,1') = \rho^{(0)}(1,1') + \Delta\rho'(1,1') = \rho^{(0)}(1,1') \\ + \sum_{i}^{\text{occ}}\sum_{a}^{\text{vir}} U_{ai}\phi_a(1)\phi_i^*(1') + \sum_{i}^{\text{occ}}\sum_{a}^{\text{vir}} U_{ai}^*\phi_a^*(1')\phi_i(1) \\ + \sum_{i}^{\text{occ}}\sum_{a}^{\text{vir}}\sum_{b}^{\text{vir}} U_{ai}^*U_{bi}\phi_a(1')\phi_b^*(1') - \sum_{i}^{\text{occ}}\sum_{j}^{\text{occ}}\sum_{a}^{\text{vir}} U_{ai}^*U_{aj}\phi_i(1')\phi_j^*(1')\end{aligned} \tag{5}$$

The expression for $\rho'(1,1')$ now makes it possible to write down the corresponding excited state Kohn–Sham energy to second order as

$$\begin{aligned}E_{\text{KS}}[\rho'(1,1')] = E_{\text{KS}}[\rho^0] + \sum_{ai} U_{ai}U_{ai}^*\left(\varepsilon_a^0 - \varepsilon_i^0\right) + \sum_{ai}\sum_{bj} U_{ai}U_{bj}^*K_{ai,bj} \\ + \frac{1}{2}\sum_{ai}\sum_{bj} U_{ai}U_{bj}K_{ai,jb} + \frac{1}{2}\sum_{ai}\sum_{bj} U_{ai}^*U_{bj}^*K_{ai,jb} + O\left[U^{(3)}\right].\end{aligned} \tag{6}$$

Here $E_{\mathrm{KS}}[\rho^0]$ is the ground state energy and "a,b" run over virtual ground state canonical orbitals whereas "i,j" run over occupied ground state canonical orbitals. Further,

$$K_{ru,tq} = K^{C}_{ru,tq} + K^{XC}_{ru,tq} \tag{7}$$

where

$$K^{C}_{ru,tq} = \int\int \phi^*_r(1)\phi_u(1)\frac{1}{r_{12}}\phi_t(2)\phi^*_q(2)dv_1 dv_2 \tag{8}$$

whereas

$$K^{XC(\mathrm{HF})}_{ru,tq} = -\int\int \phi^*_r(1)\phi_t(2)\frac{1}{r_{12}}\phi_u(2)\phi^*_q(1)dv_1 dv_2 \tag{9a}$$

for Hartree–Fock exchange correlation and

$$K^{XC(\mathrm{KS})}_{ru,tq} = \delta(m_{sr},m_{su})\delta(m_{st},m_{sq})\int \phi^*_r\left(\vec{r}_1\right)\phi_u\left(\vec{r}_1\right)\left[f^{(m_{sr},m_{st})}(\rho^0)\right]\phi_t\left(\vec{r}_1\right)\phi^*_q\left(\vec{r}_1\right)d\vec{r}_1 \tag{9b}$$

for DFT exchange correlation. In (9a) $m_{sr} = 1/2$ for a spin orbital $\phi_r(1)$ of α-spin whereas $m_{sr} = -1/2$ for a spin orbital $\phi_r(1)$ of β-spin. In addition, the kernel $f^{(\tau,\upsilon)}(\rho^0)$ is the second functional derivative of E_{XC} with respect to ρ_α and ρ_β:

$$f^{\tau,\upsilon}\left(\rho^0_\alpha,\rho^0_\beta\right) = \left(\frac{\delta^2 E_{XC}}{\delta\rho_\tau\delta\rho_\upsilon}\right)_0 \quad \tau = \alpha,\beta\ ;\ \upsilon = \alpha,\beta. \tag{10}$$

Finally for KS exchange we have the case where $\phi_u\left(\vec{r}_1\right),\phi_q\left(\vec{r}_1\right)$ have the same (α) spin whereas $\phi_r\left(\vec{r}_1\right),\phi_t\left(\vec{r}_1\right)$ are of the other (β) spin. In this case we have, according to Wang and Ziegler [67–69],

$$K^{\mathrm{KS}(XC)}_{\bar{r}u,\bar{t}q} = \frac{1}{2}\int\left[\overline{\phi}^*_r\left(\vec{r}_1\right)\phi_u\left(\vec{r}_1\right)\overline{\phi}_t\left(\vec{r}_1\right)\phi^*_q\left(\vec{r}_1\right)\right]\left[\left(\frac{1}{s^0}\left(\frac{\delta E_{XC}}{\delta\rho_\alpha}-\frac{\delta E_{XC}}{\delta\rho_\beta}\right)\right)_{(\rho^0,s^0)}\right]d\vec{r}_1 \tag{11}$$

In (11) the integration is over space and $\overline{\phi}_r\left(\vec{r}_1\right),\overline{\phi}_t\left(\vec{r}_1\right)$ are the spatial parts of orbitals with β-spin. The evaluation of $K^{\mathrm{KS}(XC)}_{\bar{r}u,\bar{t}q}$ by numerical integration might lead to numerical instabilities if $s^0 = \rho^\alpha - \rho^\alpha \approx 0$. We can, in that case, carry out a Taylor expansion of $\partial E^{\mathrm{KS}}_{XC}/\partial\rho_\alpha, \partial E^{\mathrm{KS}}_{XC}/\partial\rho_\beta$ from $\rho = \rho^\alpha + \rho^\beta$ and $s^0 = 0$. Thus

$$K^{\mathrm{KS}(XC)}_{\bar{r}u,\bar{t}q} = \frac{1}{2}\int \left[\overline{\phi}^*_r(\bar{r}_1)\phi_u(\bar{r}_1)\overline{\phi}_t(\bar{r}_1)\phi^*_q(\bar{r}_1)\right]\frac{1}{2}\left[\left(\frac{\delta^2 E_{XC}}{\delta^2\rho_\alpha}+\frac{\delta^2 E_{XC}}{\delta^2\rho_\beta}-2\frac{\delta^2 E_{XC}}{\delta\rho_\alpha\delta\rho_\alpha}\right)_{(\rho^0,s^0)}\right]dr_1$$
$$= K^{\mathrm{KS},XC}_{ru,tq} - K^{\mathrm{KS},XC}_{\bar{r}t,uq} \tag{12}$$

where $K^{\mathrm{KS},XC}_{ru,tq}, K^{\mathrm{KS},XC}_{\bar{r}t,uq}$ are defined in (9a) and (9b). The expression in (12) is numerically stable and has no singularities for $s^0 = 0$. Finally, $\varepsilon^0_i, \varepsilon^0_a$ in (6) are the ground state orbital energies of $\phi_i(1)$ and $\phi_a(1)$, respectively.

2.2 Equivalence Between Adiabatic TDDFT and Second Order Constricted Variational Density Functional Theory

In second order variational density functional theory (CV(2)-DFT) we seek points on the energy surface $E_{\mathrm{KS}}[\rho']$ such that $\Delta E_{\mathrm{KS}}[\Delta\rho'] = E_{\mathrm{KS}}[\rho'] - E_{\mathrm{KS}}[\rho^0]$ represents transition energy. Obviously, a direct optimization of $\Delta E_{\mathrm{KS}}[\Delta\rho']$ without constraints results in $\Delta E_{KS}[\Delta\rho'] = 0$ and $U = 0$. We [29] now introduce the constraint that the electron excitation must represent a change in density $\Delta\rho'$ in which one electron in (5) is transferred from the occupied space represented by $\Delta\rho_{\mathrm{occ}} = -\sum_{ija} U_{ai}U^*_{aj}\varphi_i(1')\varphi^*_j(1)$ to the virtual space represented by $\Delta\rho_{\mathrm{vir}} = \sum_{iab} U_{ai}U^*_{bi}\varphi_a(1')\varphi^*_b(1)$. Integration of $\Delta\rho_{\mathrm{occ}}$ and $\Delta\rho_{\mathrm{vir}}$ over all space affords $-\Delta q_{\mathrm{occ}} = \Delta q_{\mathrm{vir}} = \sum_{ai} U_{ai}U^*_{ai}$. We thus introduce the constraint $\sum_{ai} U_{ai}U^*_{ai} = 1$. Constructing next the Lagrangian $L = E_{\mathrm{KS}}[\rho'] + \lambda\left(1 - \sum_{ai} U_{ai}U^*_{ai}\right)$ with λ being a Lagrange multiplier and demanding that L be stationary to any real variation in U results in the eigenvalue equation

$$\left(A^{\mathrm{KS}} + B^{\mathrm{KS}}\right)\vec{U}^{(I)} = \lambda_{(I)}\vec{U}^{(I)} \tag{13a}$$

where

$$A^{\mathrm{KS}}_{ai,bj} = \delta_{ab}\delta_{ij}\left(\varepsilon^0_a - \varepsilon^0_i\right) + K^{\mathrm{KS}}_{ai,bj}; \quad B^{\mathrm{KS}}_{ai,bj} = K^{\mathrm{KS}}_{ai,jb}. \tag{13b}$$

We can now from (13a) determine the sets of mixing coefficients $\left\{\vec{U}^{(I)}; I = 1, \mathrm{occ}\times\mathrm{vir}\right\}$ which make L stationary and represent excited states. The corresponding excitation energies are given by $\lambda_{(I)}$, as can be seen by

substituting $\vec{U}^{(I)}$ into (6) and making use of the constraint and normalization condition $\vec{U}^{(I)+}\vec{U}^{(I)} = 1$ after multiplying on both sides with $\vec{U}^{(I)+}$.

Within the Tamm–Dancoff approximation [70], (13a) reduces to

$$A^{\mathrm{KS}}\vec{U}^{(I)} = \lambda_{(I)}\vec{U}^{(I)} \tag{14}$$

which is identical in form to the equation obtained from ATDDFT in its adiabatic formulation [3–9] after applying the same Tamm–Dancoff [70] approximation (ATDDFT-TD). We have recently shown [62] that CV(2)-DFT without the Tamm–Dancoff approximation is equivalent to the full adiabatic TDDFT scheme developed by Gross [3], Casida [4], and others [5–9].

2.3 *Perturbative All Order Constricted Variational Density Functional Theory*

Having determined $\vec{U}^{(I)}$ from (14) allows us [28] to turn to a discussion of how we construct the proper energy expression for excited singlet states originating from a closed shell ground state. We first consider a spin-conserving transition from a close shell ground state and assume without loss of generality that the transition takes place in the α-manifold. In this case we can write the occupied excited state KS-orbitals generated from the unitary transformation of (2a) and (2b) as [28, 71]

$$\phi_i^{'} = \cos[\eta\gamma_i]\phi_i^{o_\alpha} + \sin[\eta\gamma_i]\phi_i^{v_\alpha}; \quad i = 1, \mathrm{occ}/2 \tag{15}$$

and

$$\phi_i^{'} = \phi_i; \quad i = \mathrm{occ}/2 + 1, \mathrm{vir} \tag{16}$$

whereas the corresponding KS-determinant is given by

$$\Psi_M = \left|\phi_1^{'}\phi_2^{'}\ldots\phi_i^{'}\phi_j^{'}\ldots\phi_n^{'}\right| \tag{17}$$

Here Ψ_M represents a mixed spin-state [40] which is half singlet and half triplet. Further, $\gamma_i(i = 1, \mathrm{occ}/2)$ is a set of eigenvalues to

$$(\mathbf{V}^{\alpha\alpha})^{\dagger}(\mathbf{U}^{\alpha\alpha})(\mathbf{W}^{\alpha\alpha}) = \mathbf{1}\gamma \tag{18}$$

where γ is a diagonal matrix of dimension occ/2 whereas $\mathbf{U}^{\alpha\alpha}$ is the part of the $\mathbf{U}$ matrix which runs over the occupied $\{\phi_i; i = 1, \mathrm{occ}\}$ and virtual $\{\phi_a; a = 1, \mathrm{vir}\}$ ground state orbitals of α-spin [28, 71]. Further,

$$\phi_i^{o_\alpha} = \sum_j^{\mathrm{occ}/2} \left(\mathbf{W}^{\alpha\alpha}\right)_{ji} \phi_j \tag{19}$$

and

$$\phi_i^{v_\alpha} = \sum_a^{occ/2} \left(\mathbf{V}^{\alpha\alpha}\right)_{ai} \phi_a \tag{20}$$

Finally, η is determined in such a way that $\sum_{i=1}^{\mathrm{occ}/2} \sin^2\left[\eta\gamma_i\right] = 1$, corresponding to the constraint that exactly one electron charge is involved in the transition [28]. The orbitals defined in (19) and (20) have been referred to as Natural Transition Orbitals (NTO) [72] because they give a more compact description of the excitations than the canonical orbitals. Thus, a transition involving several $i \rightarrow a$ replacements among canonical orbitals can often be described by a single replacement $\phi_i^{o_\alpha} \rightarrow \phi_i^{v_\alpha}$ in terms of NTOs. We note again that the set in (16) is obtained from the unitary transformation (2a) and (2b) among the occupied $\{\phi_i : i = \mathrm{vir}/2 + 1, \mathrm{vir}\}$ and virtual $\{\phi_a; i = 1, \mathrm{vir}/2\}$ ground state orbitals of α-spin with $\mathbf{U}$ represented by $\mathbf{U}^{\alpha\alpha}$.

For a spin-flip transition from a closed shell ground state the unitary transformation (2a) and (2b) among the occupied ground state orbitals $\{\phi_i; i = 1, \mathrm{occ}/2\}$ of α-spin and the virtual ground state orbitals $\{\phi_a; i = \mathrm{vir}/2 + 1, \mathrm{vir}\}$ of β-spin yields the occupied excited state orbitals

$$\phi_i^{''} = \cos\left[\eta\gamma_i^{'}\right]\phi_i^{o_\alpha} + \sin\left[\eta\gamma_i^{'}\right]\phi_i^{v_\beta}\ ; i = 1, \mathrm{occ}/2 \tag{21}$$

and

$$\phi_i^{''} = \phi_i\ ;\ i = \mathrm{occ}/2 + 1, \mathrm{vir} \tag{22}$$

whereas the corresponding KS-determinant is given by

$$\Psi_T = \left|\phi_1^{''}\phi_1^{''} \ldots \phi_i^{''}\phi_j^{''} \ldots \phi_n^{''}\right| \tag{23}$$

Here Ψ_T represents a triplet state. Further, $\gamma_i (i = 1, \mathrm{occ}/2)$ are the eigenvalues to

$$\left(\mathbf{V}^{\beta\alpha}\right)^{\dagger}\left(\mathbf{U}^{\beta\alpha}\right)\left(\mathbf{W}^{\beta\alpha}\right) = \mathbf{1}\gamma' \tag{24}$$

where $\mathbf{U}^{\beta\alpha}$ is the part of $\mathbf{U}$ which runs over the virtual ground state orbitals of β-spin and occupied ground state orbitals of α-spin. Finally

$$\phi_i^{o_\alpha} = \sum_j^{\text{occ}/2} \left(\mathbf{W}^{\beta\alpha}\right)_{ji} \phi_j \tag{25}$$

and

$$\phi_i^{v_\beta} = \sum_{a=\text{vir}/2+1}^{a=\text{vir}} \left(\mathbf{V}^{\beta\alpha}\right)_{ai} \phi_a \tag{26}$$

With the excitation energy of Ψ_T given by ΔE_T and that of Ψ_M by ΔE_M, we can write the singlet transition energy as [40]

$$\Delta E_S = 2\Delta E_M - \Delta E_T \tag{27}$$

provided that $\mathbf{U}^{\alpha\alpha} = \mathbf{U}^{\beta\alpha}$. This implies that $\mathbf{V}^{\alpha\alpha} = \mathbf{V}^{\beta\alpha}$, $\mathbf{W}^{\alpha\alpha} = \mathbf{W}^{\beta\alpha}$, and $\gamma = \gamma'$. As a result, $\phi_i^{o_\alpha}$ of (19) and (25) become identical as do the spatial parts of $\phi_i^{v_\alpha}$ in (20) and $\phi_i^{v_\beta}$ in (26). Straightforward manipulations [27, 28] allow us finally to write down the mixed state transition energy to all orders in $\mathbf{U}$ in a compact and closed form as

$$\begin{aligned}
\Delta E_M = & \sum_{i=1}^{\text{occ}/2} \sin^2\left[\eta\gamma_i\right]\left(\varepsilon_{i^{v_\alpha}} - \varepsilon_{i^{o_\alpha}}\right) \\
& + \frac{1}{2}\sum_{i=1}^{\text{occ}/2}\sum_{j=1}^{\text{occ}/2} \sin^2\left[\eta\gamma_i\right]\sin^2\left[\eta\gamma_j\right]\left(K_{i^{o_\alpha}i^{o_\alpha}j^{o_\alpha}j^{o_\alpha}} + K_{i^{v_\alpha}i^{v_\alpha}j^{v_\alpha}j^{v_\alpha}} - 2K_{i^{o_\alpha}i^{o_\alpha}j^{v_\alpha}j^{v_\alpha}}\right) \\
& + \sum_{i=1}^{\text{occ}/2}\sum_{j=1}^{\text{occ}/2} \sin\left[\eta\gamma_i\right]\cos\left[\eta\gamma_i\right]\sin\left[\eta\gamma_j\right]\cos\left[\eta\gamma_j\right]\left(K_{i^{o_\alpha}i^{v_\alpha}j^{o_\alpha}j^{v_\alpha}} + K_{i^{o_\alpha}i^{v_\alpha}j^{v_\alpha}j^{o_\alpha}}\right) \\
& + 2\sum_{i=1}^{\text{occ}/2}\sum_{j=1}^{\text{occ}/2} \sin\left[\eta\gamma_i\right]\sin\left[\eta\gamma_i\right]\sin\left[\eta\gamma_j\right]\cos\left[\eta\gamma_j\right]K_{i^{v_\alpha}i^{v_\alpha}j^{o_\alpha}j^{v_\alpha}} \\
& - 2\sum_{i=1}^{\text{occ}/2}\sum_{j=1}^{\text{occ}/2} \sin\left[\eta\gamma_i\right]\sin\left[\eta\gamma_i\right]\sin\left[\eta\gamma_j\right]\cos\left[\eta\gamma_j\right]K_{i^{o_\alpha}i^{o_\alpha}j^{o_\alpha}j^{v_\alpha}}
\end{aligned} \tag{28}$$

for spin-conserving transition from a close shell ground state. More details are given in Sect. 2.4. Here the indices $i^{o_\alpha}, j^{o_\alpha}, i^{v_\alpha}$, and j^{v_α} refer to α-spin orbitals with the spatial parts $\phi_i^{o_\alpha}, \phi_j^{o_\alpha}, \phi_i^{v_\alpha}$, and $\phi_j^{v_\alpha}$, respectively. The expression for the corresponding triplet transition energy reads

$$\begin{aligned}\Delta E_T = &\sum_{i=1}^{occ/2} \sin^2\left[\eta' \gamma_i'\right](\varepsilon_{i^{v\beta}} - \varepsilon_{i^{o\alpha}}) \\ &+ \frac{1}{2}\sum_{i=1}^{occ/2}\sum_{j=1}^{occ/2} \sin^2\left[\eta' \gamma_i'\right] \sin^2\left[\eta' \gamma_i'\right]\left(K_{i^{o\alpha}i^{o\alpha}j^{o\alpha}j^{o\alpha}} + K_{i^{v\beta}i^{v\beta}j^{v\beta}j^{v\beta}} - 2K_{i^{o\alpha}i^{o\alpha}j^{v\beta}j^{v\beta}}\right) \quad (29) \\ &+ \sum_{i=1}^{occ/2}\sum_{j=1}^{occ/2} \sin\left[\eta' \gamma_i'\right] \cos\left[\eta' \gamma_i'\right] \sin\left[\eta' \gamma_j'\right] \cos\left[\eta' \gamma_j'\right] K_{i^{o\alpha}i^{v\beta}j^{o\alpha}j^{v\beta}}\end{aligned}$$

Here the indices $i^{v\beta}$ and $j^{v\beta}$ refer to β-spin orbitals with the spatial parts $\phi_i^{v\beta}$ and $\phi_i^{v\beta}$, respectively. More details are given in Sect. 2.4. From (28) and (29) we can readily express ΔE_S using (27).

In perturbative all order constricted variational DFT (P-CV(∞)-DFT) [27, 64] we make use of the **U** matrix optimized to second order according to (14), which is also the **U** obtained by ATDDFT-TD (CV(2)-DFT-TD). With this **U** we are able to generate Ψ_M of (17) and Ψ_T of (23) by means of (2a) and (2b). From that we can calculate ΔE_T and ΔE_S by means of (27)–(29).

2.3.1 Application of Perturbative All Order Constricted Variational Density Functional Theory to $\pi \rightarrow \pi^*$

We have carried out ATDDFT-TD, (CV(2)-DFT-TD), and P-CV(∞)-DFT calculations [27] on $\pi \rightarrow \pi^*$ transitions in the series of polyenes depicted in Fig. 1 using LDA. In the following we simplify the notation by referring to ATDDFT, ATDDFT-TD, CV(2)-DFT-TD, and P-CV(∞)-DFT-TD as TDDFT, TDDFT-TD, CV(2)-TD, and CV(∞)-TD, respectively, throughout Sect. 2.3.

The results are displayed in Table 1. We have divided the $\pi \rightarrow \pi^*$ transitions into a group A where each excitation is dominated by a single orbital replacement ($\gamma_{max} > 1.0$) and a group B where the excitation is best described by several orbital replacements ($\gamma_{max} < 1.0$). The group B transitions generally consist of two orbital replacements involving the HOMO → LUMO + 1 and the HOMO − 1 → LUMO transitions. It can be seen that the group B results for P-CV(∞)-TD with a root

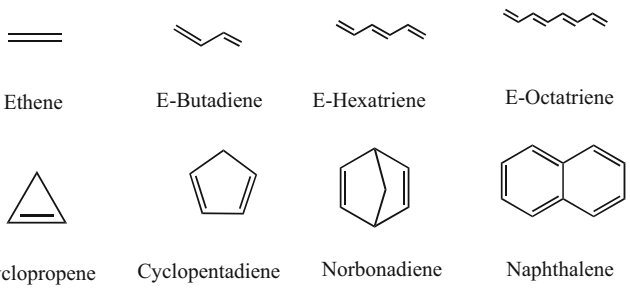

Fig. 1 Molecules used in the study of $\pi \rightarrow \pi^*$ transitions based on P-CV(∞)-DFT

Table 1 Results from TDDFT-TD and CV(∞)-TD calculations on excitation energies[a] for π to π* transitions in polyenes using LDA

	Group	State	Best[b]	TDDFT-TD[c]	CV(∞)-TD	γ_{max}[d]
Ethene	A	B_{1u}	7.80	8.44	8.39	1.177
Butadiene	A	B_u	6.18	6.16	6.10	1.174
	B	A_g	6.55	6.24	6.70	0.841
Hexatriene	B	A_g	5.09	5.03	5.36	0.787
	A	B_u	5.10	5.05	4.93	1.200
Octatetraene	B	A_g	4.47	4.17	4.42	0.799
	A	B_u	4.66	4.34	4.16	1.212
Cyclopropene	A	B_2	7.06	6.30	7.55	1.253
Cyclopentadiene	A	B_2	5.55	5.39	5.87	1.254
	B	A_1	6.31	6.05	6.45	0.809
Norbornadiene	A	A_2	5.34	4.52	5.10	1.158
	B	B_2	6.11	4.95	5.36	0.942
Naphthalene	B	B_{3u}	4.24	4.20	4.39	0.788
	A	B_{2u}	4.77	4.25	4.71	1.103
	B	B_{1g}	5.99	4.97	5.24	0.850
	B	A_g	5.87	5.80	6.02	0.854
	A	B_{2u}	6.33	6.12	6.09	1.043
	B	A_g	6.67	6.21	6.71	0.904
	B	B_{3u}	6.06	6.22	6.14	0.730
	B	B_{1g}	6.47	6.47	6.36	0.791
RMSD A[e]				0.48	0.35	
RMSD B				0.51	0.34	
RMSD A + B				0.50	0.35	

[a]Energies in eV
[b]Ab initio benchmark calculations [73]
[c]Identical to CV(2)-TD
[d]Maximum γ eigenvalue for this transition; see (18)
[e]Root mean square deviation in eV

mean square deviation (RMSD) of 0.34 eV compared to the best [73] wave function results constitute an improvement over the TDDFT-TD excitation energies with an RMSD of 0.51 eV. For the group A transitions we also note an improvement in going from TDDFT-TD with RMSD = 0.48 eV to CV(∞)-TD with RMSD = 0.35 eV. From experience so far [27, 64] it seems that CV(∞) can be used with advantage in studies of $\pi \rightarrow \pi^*$ transitions involving dyes employing simple local functionals.

2.3.2 Application of Perturbative All Order Constricted Variational Density Functional Theory to Acenes

The singlet ^1L_a and ^1L_b $\pi \rightarrow \pi^*$ excitations in linear polyacenes represent a set of benchmark excitations which have been studied extensively both experimentally

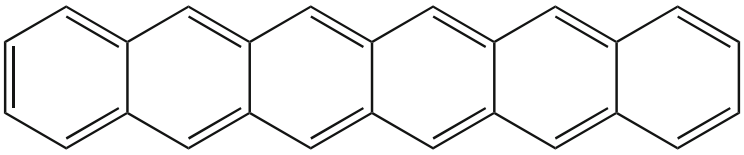

Fig. 2 Linear acenes with up to six fused rings ($n_r = 6$) considered in this study

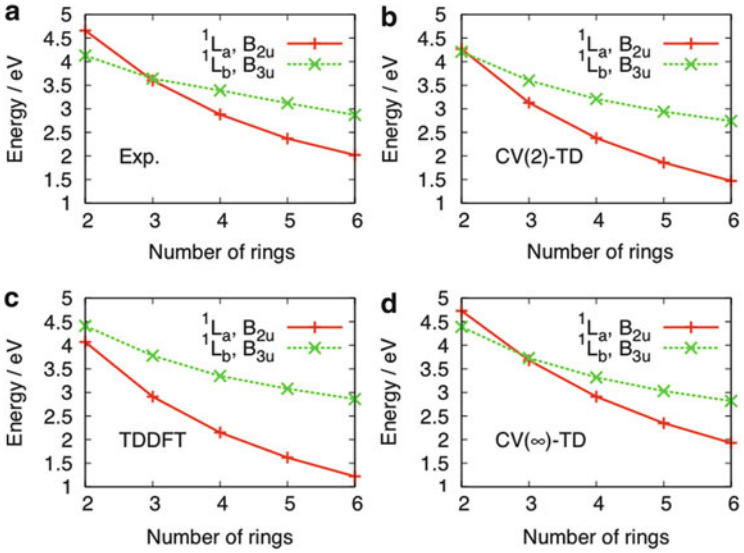

Fig. 3 Excitation energies for the ^1L_a and ^1L_b transitions in linear acenes as a function of the number of rings according to (**a**) experiment, (**b**) CV(2)-TD, (**c**) TDDFT, or (**d**) CV(∞)-TD

[74] and theoretically [75–78]. Here the acenes consist of a number (n_r) of fused benzene rings; see Fig. 2.

The distinct properties [74] of the ^1L_a and ^1L_b states for the linear acenes have already been described in the literature [75–78]. Essentially, the ^1L_a (or $^1B_{2u}$ when the x-axis corresponds to the long molecular axis state) is dominated by a single electron transition HOMO → LUMO, while the ^1L_b (or $^1B_{3u}$) state results from a combination of HOMO − 1 → LUMO and HOMO → LUMO + 1 transitions. Further, excitations to ^1L_a ($^1B_{2u}$) are short axis polarized with high intensity whereas the transitions to ^1L_b ($^1B_{3u}$) are long axis polarized with low intensity.

It follows from Fig. 3a that the experimental energy gap $\Delta E = \Delta E\left(^1B_{2u}2u\right) - \Delta E\left(^1B_{3u}3u\right)$ starts out positive at naphthalene ($n_r = 2$) with $\Delta E = 0.53$ eV before turning negative at anthracene ($n_r = 3$) where $\Delta E = 0.04$ eV. For larger linear acenes ΔE becomes increasingly negative, reaching $\Delta E = 0.85$ eV at hexacene. Thus, experimentally, $\Delta E(^1B_{2u})$ is seen to drop faster in energy than $\Delta E(^1B_{3u})$.

Table 2 Root mean square deviations ([d]RMSD) from experiment for ^1L_a and ^1L_b $\pi \rightarrow \pi^*$ excitations calculated by TDDFT, TDDFT-TD and CV(∞)-TD for linear and nonlinear acenes using LDA

	RMSD $^1B_{2u}$ (^1L_a)			RMSD $^1B_{3u}$ (^1L_b)		
Systems	TDDFT	TDDFT-TD[a]	CV(∞)-TD	TDDFT	TDDFT-TD[a]	CV(∞)-TD
Linear[b]	0.71	0.49	0.06	0.14	0.13	0.13
Nonlinear[c]	0.52	0.40	0.24	0.16	0.15	0.19

[a]Identical to CV(2)-TD
[b]Linear acenes of Fig. 2
[c]Nonlinear acenes of Fig. 4
[d]Ev

The ordering of the calculated CV(2)-TD (TDDFT-TD) excitation energies based on LDA(VWN) is correct for naphthalene as well as for all other linear acenes, although the gap differs from the experimental ΔE by almost 0.4 eV for naphthalene, anthracene, and hexacene. This difference is smaller for naphthacene and pentacene (Fig. 3b). It can be seen that the main contribution to this deviation comes from the underestimation of $\Delta E(^1B_{2u})$ Thus, the root mean square deviation (RMSD) value for $\Delta E(^1B_{2u})$ is 0.49 eV, while it is only 0.13 eV for $\Delta E(^1B_{3u})$; see Table 2.

As for the TDDFT results based on LDA(VWN), the deviation from the experimental gaps is larger in absolute terms and the calculated ΔE has the wrong sign for naphthalene (Fig. 3c). It happens because the $\Delta E(^1B_{2u})$ values for TDDFT are lower than those for CV(2)-TD while the $\Delta E(^1B_{3u})$ estimates for TDDFT are higher than for CV(2)-TD. As a result, the RMSD value for $\Delta E(^1B_{2u})$ increases for TDDFT by approximately 0.2 eV and reaches 0.71 eV; see Table 2. On the other hand, on average the TDDFT estimate of $\Delta E(^1B_{3u})$ is as accurate as for CV(2)-TD (TDDFT-TD). Thus, the TDDFT $\Delta E(^1B_{3u})$ values for naphthacene, pentacene, and hexacene are closer to experiment than those from CV(2)-TD while the opposite is true for naphthalene and anthracene. The RMSD value for TDDFT is 0.14 eV compare to 0.13 eV for CV(2)-TD; see Table 2.

It follows from the discussion given above that neither CV(2)-TD nor TDDFT are able to give a quantitative description of ΔE as a function of n_r with LDA, in line with previous TDDFT studies [75–78], using both pure density functionals and hybrids. The source of the error is in all cases primarily $\Delta E(^1B_{2u})$ which is too low compared to experiment. However, $\Delta E(^1B_{3u})$ is also seen to be slightly too high.

We note finally from Table 3 and Fig. 3d that the CV(∞)-TD results using LDA [64] are in excellent agreement with experiment for both $\Delta E(^1B_{3u})$ and $\Delta E(^1B_{2u})$ throughout the range of linear acenes (1–6 of Fig. 4). The RMSD for $\Delta E(^1B_{2u})$ is 0.06 eV whereas that for $\Delta E(^1B_{3u})$ is 0.13 eV; see Table 2. Thus, CV(∞)-TD clearly represents an improvement over TDDFT and CV(2)-TD for LDA. The improvement is, as anticipated, most noticeable for $\Delta E(^1B_{2u})$ where the RMSD was 0.71 eV for TDDFT and 0.49 eV for CV(2)-TD. For $\Delta E(^1B_{3u})$ all three methods have a similar RMSD.

We have extended [64] our benchmark calculations to include the 15 nonlinear acenes shown in Fig. 4. The RSMDs for the singlet transition energies involving ^1L_a

Table 3 CV(∞)-TD singlet excitation energies (in eV) for linear acenes with LDA

Number of rings	Experiment[a]			CV(∞)-TD		
	$^1B_{2u}$	$^1B_{3u}$	ΔE^b	$^1B_{2u}$	$^1B_{3u}$	ΔE^b
2	4.66	4.13	0.53	4.73	4.39	0.34
3	3.60	3.64	−0.04	3.68	3.73	−0.05
4	2.88	3.39	−0.51	2.91	3.32	−0.41
5	2.37	3.12	−0.75	2.35	3.03	−0.68
6	2.02	2.87	−0.85	1.93	2.82	−0.89

[a]Platt [74]
[b]$\Delta E = \Delta E(^1B_{2u}) - \Delta E(^1B_{3u})$

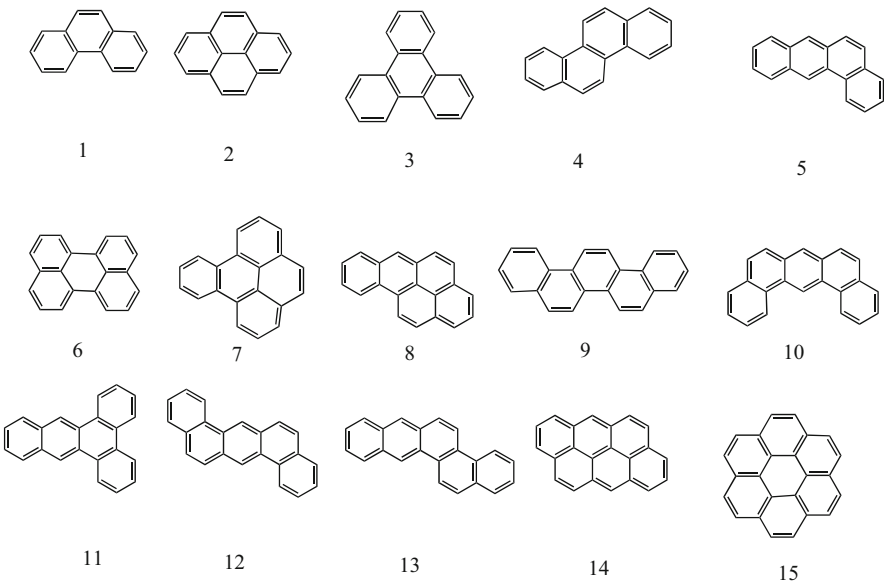

Fig. 4 Nonlinear acenes with up to six fused rings ($n_r = 6$) considered in this study

and ^1L_b are given in Table 2 for TDDFT, CV(2)-TD, and CV(∞)-TD based on LDA. ^1L_a CV(∞)-TD with an RMSD of 0.24 eV is seen to perform better than CV (2)-TD (RMSD = 0.40 eV) and especially TDDFT (0.52 eV). In fact our results are of a similar quality to the best results obtained by long-range corrected (LRC) functionals [79]. We note again that the ^1L_a transitions involves a single HOMO → LUMO orbital displacement with $\gamma_i = \pi/2$. For ^1L_b all three methods perform equally well with RMSDs of 0.16 eV (TDDFT), 0.15 eV(CV(2)-TD), and 0.19 eV (P-CV(∞)-DFT), respectively. It is interesting to note that the LRC-functionals [79] in this case perform much more poorly with RMSDs around 0.4 eV. Thus, CV(∞)-TD at the simple LDA level is the only scheme of the methods discussed here which gives a balanced description of $\pi \rightarrow \pi^*$ transitions involving a single orbital displacement (^1L_a) and $\pi \rightarrow \pi^*$ transitions with more than one displacement.

For the CV(∞)-scheme we note that the singlet excitation energy for a transition involving a single promotion $i \rightarrow a$ such as $^1A_{1g}1g \rightarrow {}^1B_{2u}2u$ according to (27)–(29) has the simple form [27]:

$$\Delta E_S^{CV(\infty)}(i \rightarrow a) = \varepsilon_a - \varepsilon_i + \left(\frac{1}{2}K_{aaaa} + \frac{1}{2}K_{iiii} + 2K_{aaii} - K_{i\overline{i}a\overline{a}}\right) \tag{30}$$

Here i is the HOMO π and a the LUMO π^* in the current study. Further, a bar "‾" indicates an orbital of β-spin. For CV(2)-TD we obtain for the same transition according to (14) and (27)

$$\Delta E_S^{CV(2)}(i \rightarrow a) = \varepsilon_a - \varepsilon_i + 2K_{aiai} - K_{\overline{a}i\overline{a}i} \tag{31}$$

For HF these two expressions are identical [27] because $K_{aaaa} = K_{iiii} = 0$ and $K_{aiai} = -K_{aaii}$. However, for any of the popular functionals this is not the case. Thus, the two expressions give rise to different excitation energies for the same functional. In the study at hand [27] on the $^1A_{1g}1g \rightarrow {}^1B_{2u}2u$ transition the sum of the K-integrals in (30) is larger than the sum of the K-integrals in (31) by 0.5 eV, giving rise to the better performance of CV(∞)-TD compared to CV(2)-TD for the $^1A_{1g}1g \rightarrow {}^1B_{2u}2u$ transition. We note that acenes have also been well described by the variational DFT-based spin-restricted ensemble referenced Kohn–Sham (REKS) method [57].[1]

2.4 *Self-Consistent All Order Constricted Variational Density Functional Theory*

Using the U matrix from TDDFT-TD or CV(2)-TD to calculate ΔE_M of (28) or ΔE_T of (29), as is done in P-CV(∞)-TD, might be a good approximation. However, ultimately, one would want to use a U matrix which actually minimizes ΔE_M of (28) or ΔE_T of (29). Such a procedure leads us to self-consistent CV(∞)-DFT (SCF-CV(∞)-DFT) [27] which we discuss next. We note that the **U** matrix can also be organized as a vector $\vec{U}$ with pairs "ai" of occupied and virtual orbitals as running numbers. The two formulations are used interchangeably in the following.

From the occupied excited state orbitals of (17) and (23) we can express the electron density and spin matrices.[2,3] Starting with a spin-conserving transition from a close shell ground state, we can, without loss of generality, assume that it

[1] See the chapter "Ensemble DFT approach to excited states of strongly correlated molecular systems" by M. Filatov.

[2] See Sect. 3.1 from part S1 of supporting information in Ziegler et al. [27].

[3] See Sect. 3.3 from part S1 of supporting information in Ziegler et al. [27].

takes place between orbitals of α-spin. Thus, for such a spin-conserving transition, the excited state orbitals $\phi_i^{'} = \cos[\eta\gamma_i]\phi_i^{o_\alpha} + \sin[\eta\gamma_i]\phi_i^{v_\alpha}$ (15) are obtained by the unitary transformation at (2a) and (2b) to all orders involving the part of the **U** matrix ($\mathbf{U}^{\alpha\alpha}$) which, according to (1), mixes occupied ground state orbitals of α-spin with virtual ground state orbitals of α-spin. We can now write (see footnote 3) the change in density within the α-manifold caused by the excitation as

$$\begin{aligned}\Delta\rho_M(1,1^{'}) = &\sum_j^{\text{occ}/2} \sin^2\left[\eta^\alpha\gamma_j^\alpha\right]\left[\varphi_j^{v_\alpha}(1')\varphi_j^{v_\alpha}(1) - \varphi_j^{o_\alpha}(1')\varphi_j^{o_\alpha}(1)\right] \\ &+ \sum_j^{\text{occ}/2} \sin\left[\eta^\alpha\gamma_j^\alpha\right]\cos\left[\eta^\alpha\gamma_j^\alpha\right]\left[\varphi_j^{v_\alpha}(1)\varphi_j^{o_\alpha}(1') + \varphi_j^{v_\alpha}(1')\varphi_j^{o_\alpha}(1)\right]\end{aligned} \tag{32a}$$

In (32a) the scaling factor η^α is introduced to ensure that $\Delta\rho^{\alpha(\infty)}(1,1')$ represents the transfer of a single electron from the occupied orbital space density $-\sum_j^{\text{occ}/2} \sin^2\left[\eta^\alpha\gamma_j^\alpha\right]\varphi_j^{o_\alpha}(1')\varphi_j^{o_\alpha}(1)$ to the virtual orbital space density $\sum_j^{\text{occ}/2} \sin^2\left[\eta^\alpha\gamma_j^\alpha\right]\varphi_j^{v_\alpha}(1')\varphi_j^{v_\alpha}(1)$ or

$$\sum_j^{\text{occ}/2} \sin^2\left[\eta^\alpha\gamma_j^\alpha\right] = 1 \tag{32b}$$

Here the constraint of (32b) is a generalization of the corresponding second order constraint $\sum_{ai} U_{ai}U_{ai} = 1$ used to derive (14). The change in density $\Delta\rho^{\alpha(\infty)}(1,1')$ now allows us to write the excitation energy for the spin conserving excitation within the α-manifold as [27]

$$\begin{aligned}\Delta E_M &\equiv E_{\text{KS}}[\rho^0/2 + \Delta\rho_M, \rho^0/2] - E_{\text{KS}}[\rho^0/2, \rho^0/2] \\ &= \int F_{\text{KS}}\left[\rho^0/2 + 1/2\Delta\rho_M, \rho^0/2)\right]\Delta\rho_M\end{aligned} \tag{33}$$

Here the right hand side of (33) is derived by Taylor expanding [80] $E_{\text{KS}}[\rho^0/2 + \Delta\rho_M, \rho^0/2]$ and $E_{\text{KS}}[\rho^0/2, \rho^0/2]$ from the intermediate point $(\rho^0/2 + \Delta\rho_M/2, \rho^0/2)$. Further, $F_{\text{KS}}(\rho^0/2 + \Delta\rho_M/2, \rho^0/2)$ is a Kohn-Sham Fock operator defined with respect to the intermediate point. The expression in (33) is exact to third order in $\Delta\rho_M$ which is usually accurate enough [80]. However, its accuracy can be extended to any desired order [80]. Taylor expanding $F_{\text{KS}}(\rho^0/2 + \Delta\rho_M/2, \rho^0/2)$ to second order in $\Delta\rho_M$ finally affords ΔE_M of (28) (see footnotes 2 and 3). The expression for ΔE_T of (29) can be derived along similar routes.[4,5]

[4] See Sect. 3.2 from part S1 of supporting information in Ziegler et al. [27].

[5] See Sect. 3.4 from part S1 of supporting information in Ziegler et al. [27].

2.4.1 Energy Gradient in SCF-CV(∞)-DFT

We now find vectors $\vec{U}^{(I)}$ which optimize ΔE_M and ΔE_T. In either case there are several which we order in terms of increasing energy with $I = 1, 2\ldots$. To this end, we need the energy gradient with respect to variations in $\vec{U}$. Considering first a spin-conserving transition[6] between orbitals of α-spin, we take as a starting point $\mathbf{U}^{\alpha\alpha}$ which generates $\phi_i' = \cos\left[\eta^\alpha \gamma_i^\alpha\right]\phi_i^{o_\alpha} + \sin\left[\eta^\alpha \gamma_i^\alpha\right]\phi_i^{v_\alpha}$ (15) the elements in $\vec{U}_{(2)}^{(I)} = \vec{U}^{(I)}$ which have been found by solving (14) for a spin conserving transition within the CV(2)-TD (TDDFT-TD) approximation for the Ith state. To the vector $\vec{U}^{(I)}$ corresponds the matrix $\tilde{\mathbf{U}}^{0,\alpha\alpha}$ and the set $\left\{\tilde{\gamma}_k^{\alpha,0}; k = 1, \mathrm{occ}\right\}$. Next, scaling $\tilde{\mathbf{U}}^{0,\alpha\alpha}$ and $\left\{\tilde{\gamma}_k^{\alpha,0}; k = 1, \mathrm{occ}\right\}$ by η^α such that $\sum_j^{\mathrm{occ}/2} \sin^2\left[\eta^\alpha \gamma_j^\alpha\right] = 1$ affords $\mathbf{U}^{0,\alpha\alpha} = \eta^\alpha \tilde{\mathbf{U}}^{0,\alpha\alpha}$ and $\left\{\gamma_k^{\alpha,0} = \eta^\alpha \tilde{\gamma}_k^{\alpha,0}; k = 1, \mathrm{occ}\right\}$ where now $\sum_j^{\mathrm{occ}/2} \sin^2\left[\eta^\alpha \gamma_j^\alpha\right] = 1$. The matrix $\tilde{\mathbf{U}}^{0,\alpha\alpha}$ is obtained from a CV(2)-TD (TDDFT-TD) calculation where $\mathbf{U}^{\alpha\alpha}$ and $-\mathbf{U}^{\alpha\alpha}$ afford the same energy according to (14). However, in CV(∞) with the energy expression given by (28), the sign matters through the terms containing cos $[\eta^\alpha \gamma_i^\alpha]sin[\eta^\alpha \gamma_i^\alpha]$. As we are dealing with a variational approach, we must pick the sign affording the lowest energy. The same considerations apply to the P-CV(∞)-DFT approach.

Next, a Taylor expansion of ΔE_M in (33) from $\mathbf{U}^{0,\alpha\alpha}$ to $\mathbf{U}^{\alpha\alpha} = \mathbf{U}^{0,\alpha\alpha} + \Delta\mathbf{U}^{\alpha\alpha}$ affords

$$\begin{aligned}\Delta E_M(\mathbf{U}^{\alpha\alpha}) &= E_M\left(\mathbf{U}^{0,\alpha\alpha}\right) + \sum_{ai}\left(\frac{d\Delta E_M}{d\Delta U_{ai}^{\alpha\alpha}}\right)_0 \Delta U_{ai}^{\alpha\alpha} \\ &+ \frac{1}{2}\sum_{ai}\sum_{bj}\left(\frac{d^2\Delta E_M}{d\Delta U_{ai}^{\alpha\alpha} d\Delta U_{bj}^{\alpha\alpha}}\right)_0 \Delta U_{ai}^{\alpha\alpha}\Delta U_{bj}^{\alpha\alpha} \\ &= \Delta E_M\left(\mathbf{U}^{0,\alpha\alpha}\right) + \sum_{ai} g_{ai}^{\alpha,e}\Delta U_{ai}^{\alpha\alpha} + \frac{1}{2}\sum_{ai}\sum_{bj} H_{ai,bj}^{\alpha,\alpha}\Delta U_{ai}^{\alpha\alpha}\Delta U_{bj}^{\alpha\alpha} + O^{(3)}[\Delta\mathbf{U}].\end{aligned} \tag{34}$$

A component of the gradient $g_{ai}^{\alpha,e}$ evaluated at $\mathbf{U}^{0,\alpha\alpha}$ reads

[6] See Sect. 4.1 from part S1 of supporting information in Ziegler et al. [27].

$$\begin{aligned}\overrightarrow{g}^{\alpha,e}_{ai}\left(U^{0,\alpha\alpha}\right) &= \left(\frac{d\Delta E_M}{d\Delta U^{\alpha\alpha}_{ai}}\right)_0 = \left(\frac{\delta\Delta E_M}{\delta\rho^\alpha}\right)_0\left(\frac{d\Delta\rho^\alpha}{d\Delta U^{\alpha\alpha}_{ai}}\right)_0 \\ &= \int F_{\mathrm{KS}}\left[\rho^0/2+1/2\Delta\rho^\alpha_M,\rho^0/2\right]\left(\frac{\partial\Delta\rho^\alpha_M}{dU^{\alpha\alpha}_{ai}}\right)_0 dv_1,\end{aligned} \tag{35}$$

Here $\Delta U^{\alpha\alpha}_{ai}$ is the change in $U^{\alpha\alpha}_{ai}$ in going from $U^{0,\alpha\alpha}_{ai}$ and $\Delta\rho^\alpha$ is the corresponding change in ρ^α. The subscript "0" in (35) indicates that the derivatives are evaluated at $U^{\alpha\alpha}_{ai}=U^{0,\alpha\alpha}_{ai}$. The calculation of $\overrightarrow{g}^{\alpha,e}_{ai}\left(U^{0,\alpha\alpha}\right)$ in (35) requires closed form expressions for $d\Delta\rho^\alpha/d\Delta U^{\alpha\alpha}_{ai}$ (see footnote 6).[7]

2.4.2 Optimization of U in SCF-CV(∞)-DFT

With the evaluation of $\overrightarrow{g}^{\alpha,e}_{ai}\left(\mathbf{U}^{0,\alpha\alpha}\right)$ we can now begin an iterative process from $\mathbf{U}^{0,\alpha\alpha}$ generated by $\overrightarrow{U}^{(I)}_{(2)}$ to the optimal $\mathbf{U}^{\alpha\alpha}$ matrix where $\Delta U^{\alpha\alpha}=0$. A differentiation of (35) by $\Delta\mathbf{U}^{\alpha\alpha}$ affords

$$\overrightarrow{g}^{e,\alpha}\left(\mathbf{U}^{0,\alpha\alpha}\right)+\mathbf{H}^{\alpha\alpha}\left(\mathbf{U}^{0,\alpha\alpha}\right)\Delta\mathbf{U}^{\alpha\alpha}=0 \tag{36}$$

from which we can find the next $\mathbf{U}^{\alpha\alpha}$. In the initial steps where $\left|\overrightarrow{\Delta U}^{\alpha\alpha}\right|\gg\delta_{\mathrm{tresh1}}$ the Hessian is calculated approximately by assuming that $\mathbf{H}^{\alpha\alpha}\left(\mathbf{U}^{0,\alpha\alpha}\right)=\varepsilon^D$ with $\left(\varepsilon^D\right)_{ai,bj}=\delta_{ij}\delta_{ab}(\varepsilon_a-\varepsilon_i)$. Here ε_i, ε_a are the energies of the occupied and virtual ground state orbitals, respectively. We thus get for each new step

$$\overrightarrow{\Delta U}^{\alpha\alpha}=\left(\varepsilon^D\right)^{-1}\overrightarrow{g}^{e,\sigma}\left(\mathbf{U}^{0,\alpha\alpha}\right) \tag{37}$$

If $\sum_j^{\mathrm{occ}/2}\sin^2\left[\eta^\alpha\gamma^\alpha_j\right]$ resulting from $\widetilde{\mathbf{U}}^{0,\alpha\alpha}=\mathbf{U}^{0,\alpha\alpha}+\Delta\mathbf{U}^{\alpha\alpha}$ does not satisfy (32b), we introduce a new η^α scaling so that $\sum_j^{\mathrm{occ}/2}\sin^2\left[\eta^\alpha\gamma^\alpha_j\right]$ constructed from $\widehat{\mathbf{U}}^{0,\alpha\alpha}=\eta^\alpha\widetilde{\mathbf{U}}^{0,\alpha\alpha}$ satisfies (32b). After that we finally ensure that $^{0,\alpha\alpha}$ satisfies $Tr\left(\widehat{U}^{0,\alpha\alpha}U^{K,\alpha\alpha}\right)=0$ for the excited states $K=1,\mathrm{I}-1$ which are below the excited state I for which we are optimizing $\mathbf{U}$. This is done by introducing the projection

$$\mathbf{U}^{0,\alpha\alpha}=\widehat{\mathbf{U}}^{0,\alpha\alpha}-\sum_{k=1}^{I-1}U^{K,\alpha\alpha}Tr\left(\mathbf{U}^{K,\alpha\alpha+}\widehat{\mathbf{U}}^{0,\alpha\alpha}\right)/Tr\left(\mathbf{U}^{K,\alpha\alpha+}\mathbf{U}^{K,\alpha\alpha}\right) \tag{38}$$

[7] See Sect. 3.0 from part S2 of supporting information in Ziegler et al. [27].

After that, we go back to (37) for a new step with $\mathbf{U}^{0,\alpha\alpha}$ defined in (38). When $\delta_{\text{tresh1}} \geq \left|\vec{\Delta U}^{\alpha\alpha}\right| \gg \delta_{\text{tresh2}}$, the iterative procedure is resumed by the help of the conjugated gradient technique described by Pople et al. [81]. It is not required in this procedure explicitly to know the Hessian. Instead, use is made of the fact that

$$\mathbf{H}^{\alpha\alpha}\left(\mathbf{U}^{0,\alpha\alpha}\right)\Delta\mathbf{U}^{\alpha\alpha} = \vec{g}^{e,\alpha}\left(\mathbf{U}^{0,\alpha\alpha} + \Delta\mathbf{U}\right) - \vec{g}^{e,\alpha}\left(\mathbf{U}^{0,\alpha\alpha}\right) + O^{[3]}(\Delta\mathbf{U}) \tag{39}$$

The value for δ_{tresh1} is typically 10^{-2} whereas $\delta_{\text{tresh2}} = 10^{-4}$. Convergence is obtained when the threshold δ_{tresh2} is reached. Typically 20–30 iterations are required to reach δ_{tresh1} and 5–10 to reach δ_{tresh2}. We have also attempted more advanced Hessians for the first part of the optimization, such as the one suggested by Fletcher [82] and implemented by Fischer and Almlöf [83]. However, it was found to be less robust than the simple procedure in (37). The optimization procedure outlined here for spin-conserving transitions can readily be formulated for spin-flip transitions [27].

2.4.3 Application of SCF-CV(∞)-DFT

We have applied SCF-CV(∞)-DFT to a number of $n_\sigma \rightarrow \pi^*$ transitions [63] where an electron is moved from an occupied lone-pair orbital n_σ to a virtual π^* orbital in the sample of molecules shown in Fig. 5. We present the results in Table. 4. For the sample of $n_\sigma \rightarrow \pi^*$ transitions studied here it can be seen that the perturbative P-CV (∞)-DFT approach with an RMSD of 1.14 eV is inadequate and one would hope that a full optimization of **U** would improve the RMSD. In fact, applying SCF-CV (∞) with complete optimization of **U** drops the RMSD to 0.50 eV, which is still poorer than CV(2)-TD (TDDFT-TD) with RMSD = 0.33 eV. At this point it is important to note that all the excitations in Table 4 can be represented by a single orbital replacement $n_\sigma \rightarrow \pi^*$. However, in going from P-CV(∞)-DFT to SCF-CV (∞) the π^* orbital is modified, leading to a lowering of the excitation energy and a reduction of RMSD.

On the other hand, all the other orbitals remain in P-CV(∞)-DFT and SCF-CV (∞) "frozen" as they are in the ground state. That this is a severe approximation can be seen from the ΔSCF results in Table 4 where RMSD = 0.32 eV. In the ΔSCF scheme we optimize not only n_σ and π^* but also all other occupied orbitals in the excited state with respect to the $(n_\sigma)^1(\pi^*)^1$ configuration. It is thus obvious that we must carry out a similar relaxation. This is done next in our SCF-CV(∞)-DFT scheme where we introduce full orbital relaxation on top of optimizing **U** (SCF-CV (∞)-DFT.

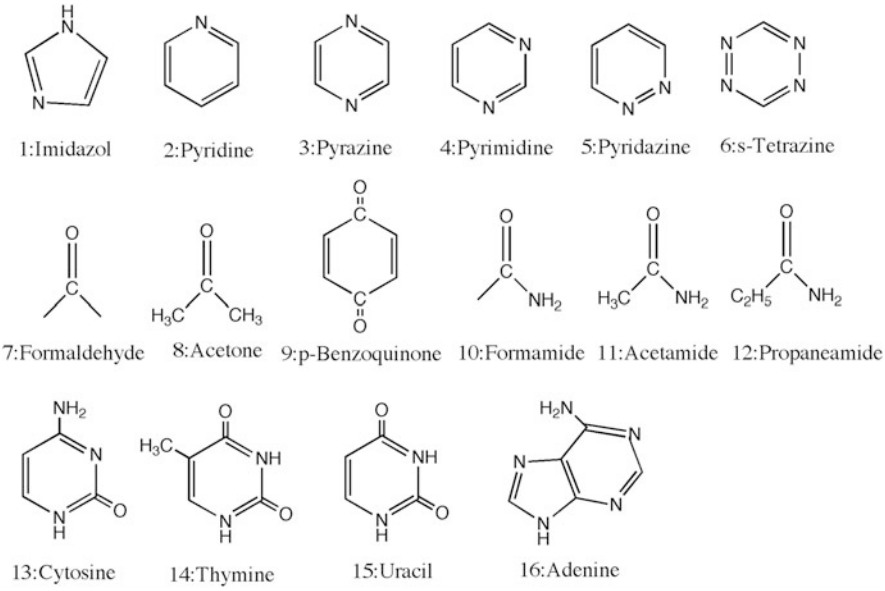

Fig. 5 Sample of molecules used in the study of $n_\sigma \rightarrow \pi^*$ transitions [26]

2.5 *Self-Consistent All Order Constricted Variational Density Functional Theory with Orbital Relaxation*

In the description of the excited state by the SCF-CV(∞)-DFT scheme all occupied β-orbitals are unchanged (frozen) from the ground state and the same is the case for a number of α-orbitals which do not directly participate in the transition. Thus in the case of the $n_\sigma \rightarrow \pi^*$ transitions, all α-orbitals other than n_σ, π^* are frozen. To remedy this, we allow in the RSCF-CV(∞)-DFT [26] scheme for a relaxation to second order in the mixing matrix $R^{\sigma\sigma}(\sigma = \alpha, \beta)$ of all occupied orbitals in the excited state [26]. Thus,

$$\psi_i^\sigma(1) \rightarrow \phi_i^\sigma(1) + \sum_c^{\mathrm{vir}/2} R_{ci}^{\sigma\sigma}\phi_c^\sigma(1) - \frac{1}{2}\sum_c^{\mathrm{vir}/2}\sum_k^{\mathrm{occ}/2} R_{ci}^{\sigma\sigma}R_{ck}^{\sigma\sigma}\phi_k^\sigma(1) + O^{(3)}[R^\sigma] \qquad (40a)$$

$$\psi_a^\sigma(1) \rightarrow \phi_a^\sigma(1) - \sum_k^{\mathrm{vir}/2} R_{ak}^{\sigma\sigma}\phi_k^\sigma(1) - \frac{1}{2}\sum_c^{\mathrm{vir}/2}\sum_k^{\mathrm{occ}/2} R_{ak}^{\sigma\sigma}R_{ck}^{\sigma\sigma}\phi_c^\sigma(1) + O^{(3)}[R^{\sigma\sigma}] \qquad (40b)$$

Replacing in (2a) the matrix $\tilde{\mathbf{U}}$ which combines occupied and virtual orbitals of the unrelaxed set $\{\phi_q; q = 1, \mathrm{occ} + \mathrm{vir}\}$ with the corresponding matrix U which mixes the occupied and virtual orbitals of the relaxed basis $\{\psi_q; q = 1, \mathrm{occ} + \mathrm{vir}\}$ leads to the unitary transformation

Table 4 Vertical singlet excitation energies[a] in $n \rightarrow \pi^*$ transitions based on B3LYP

Molecule	State	Best[b]	CV(2)[c]	P-CV(∞)[c]	SCF-CV(∞)	RSCF-CV(∞)	ΔSCF
1	A″	6.81	5.38	6.80	6.86	5.86	5.76
2	B_1	4.59	4.92	6.01	5.34	4.91	4.69
	A_2	5.11	5.17	7.20	6.26	5.10	5.15
3	B_{3u}	3.95	4.09	4.08	3.99	3.88	3.85
	A_u	4.81	4.74	5.49	5.30	4.52	4.63
	B_{2g}	5.56	5.67	5.92	5.81	5.56	5.48
	B_{1g}	6.6	6.40	7.92	7.78	6.20	6.38
4	B_1	4.55	4.37	4.94	4.72	4.19	4.14
	A_2	4.91	4.68	5.50	5.29	4.46	4.54
5	B_1	3.78	3.74	4.50	3.99	3.64	3.55
	A_2	4.31	4.26	5.75	5.29	3.96	4.15
	A_2	5.77	5.55	5.93	5.67	5.44	5.35
6	B_{3u}	2.29	2.41	2.43	2.30	2.11	2.15
	A_u	3.51	3.59	4.13	4.02	3.38	3.48
	B_{1g}	4.73	4.88	4.89	4.73	4.53	4.56
	A_u	5.5	5.20	5.22	5.16	4.92	4.96
	B_{2g}	5.2	5.40	5.34	5.31	5.16	5.17
7	A_2	3.88	3.93	4.53	4.30	3.53	3.52
8	A_2	4.4	4.41	5.19	4.84	4.01	4.02
9	B_{1g}	2.76	2.54	2.78	2.62	2.52	2.40
	A_u	2.77	2.69	3.15	2.97	2.72	2.55
	B_{3u}	5.64	5.47	6.82	6.18	5.40	5.40
10	A″	5.63	5.58	6.85	6.42	5.32	5.28
11	A″	5.69	5.59	6.94	6.43	5.33	5.31
12	A″	5.72	5.60	6.94	6.37	5.33	5.34
13	A″	4.87	4.78	7.56	5.90	4.92	4.83
	A″	5.26	5.17	7.32	6.43	5.58	–[d]
14	A″	4.82	4.74	6.75	5.73	4.78	4.59
	A″	6.16	5.63	6.66	6.64	5.96	5.82
15	A″	4.80	4.66	6.83	5.74	4.75	4.54
	A″	6.10	5.75	8.03	6.75	5.84	6.07
	A″	6.56	5.85	6.88	6.76	6.15	–[d]
16	A″	5.12	5.01	5.86	5.52	4.85	4.91
	A″	5.75	5.49	6.66	6.02	5.80	5.63
	RMSD		0.33	1.14	0.50	0.32	0.32

[a]Energies in eV
[b]Theoretical best estimates are from Schreiber et al. [73]
[c]Tamm-Dancoff approximation [70]
[d]Did not converge

$$Y\begin{pmatrix}\psi_{\text{occ}}\\ \psi_{\text{vir}}\end{pmatrix}=\mathrm{e}^{U}\begin{pmatrix}\psi_{\text{occ}}\\ \psi_{\text{vir}}\end{pmatrix}=\left(\sum_{m=0}^{\infty}\frac{U^m}{m!}\right)\begin{pmatrix}\psi_{\text{occ}}\\ \psi_{\text{vir}}\end{pmatrix}=\begin{pmatrix}\psi'_{\text{occ}}\\ \psi'_{\text{vir}}\end{pmatrix} \tag{41}$$

in which the sets of relaxed occupied $\{\psi_i; i=1,\text{occ}\}$ and virtual $\{\psi_a; a=1,\text{vir}\}$ ground state (reference) KS-orbitals are converted into the resulting sets $\{\psi'_i; i=1,\text{occ}\}$ and $\{\psi'_a; a=1,\text{vir}\}$ of relaxed occupied and virtual excited state orbitals, respectively. It should be noted that the relaxed orbital set is orthonormal to second order in **R**.

We now obtain for a spin conserving transition the excited state KS determinant which can be written as

$$\Psi_M=\left|\psi'_1\psi'_1\ldots\psi'_i\psi'_j\ldots\psi'_n\right| \tag{42}$$

The corresponding change in density $\Delta\rho_M$ expanded in terms of the unrelaxed ground state orbitals takes the form

$$\Delta\rho_M=\Delta\rho_M(U^{\alpha\alpha})+\Delta\rho_M^R \tag{43}$$

where

$$\begin{aligned}\Delta\rho_M(\mathbf{U}^{\alpha\alpha})=&\sum_{a}^{\text{vir}(\alpha)}\sum_{i}^{\text{occ}(\alpha)}\Delta P_{ai}(\mathbf{U}^{\alpha\alpha})\left[\phi_a^{\alpha}(1')\phi_i^{\alpha}(1)+\phi_a^{\alpha}(1')\phi_i^{\alpha}(1)\right]\\&+\sum_{ab}^{\text{vir}(\alpha)}\Delta P_{ab}(\mathbf{U}^{\alpha\alpha})\phi_a^{\alpha}(1')\phi_b^{\alpha}(1)+\sum_{ij}^{\text{occ}(\alpha)}\Delta P_{ij}(\mathbf{U}^{\alpha\alpha})\phi_i^{\alpha}(1')\phi_j^{\alpha}(1)\end{aligned} \tag{44}$$

is the change in density caused by $\mathbf{U}^{\alpha\alpha}$ alone and equivalent to (32a) but expressed in terms of unrelaxed ground state orbitals. On the other hand

$$\begin{aligned}\Delta\rho_M^R=&\sum_{\sigma}^{\alpha,\beta}\sum_{a}^{\text{vir}(\sigma)}\sum_{i}^{\text{occ}(\sigma)}T_{ai}^{(1)\sigma\sigma}\left[\phi_a^{\alpha}(1')\phi_i^{\alpha}(1)+\phi_a^{\alpha}(1')\phi_i^{\alpha}(1)\right]\\&+\sum_{ab}^{\text{vir}(\sigma)}T_{ab}^{(2)\sigma\sigma}\phi_a^{\sigma}(1')\phi_b^{\sigma}(1)+\sum_{ij}^{\text{occ}(\sigma)}T_{ij}^{(2)\sigma\sigma}\phi_i^{\sigma}(1')\phi_j^{\sigma}(1)\end{aligned} \tag{45}$$

is the change in density caused by the relaxation. Here

$$T_{ai}^{(1)\alpha\alpha}=R_{ai}^{\alpha\alpha}+\sum_{j}^{\text{occ}(\alpha)}\Delta P_{ij}^{\alpha\alpha}R_{aj}^{\alpha\alpha};\quad T_{ai}^{(1)\beta\beta}=R_{ai}^{\beta\beta} \tag{46a}$$

$$
\begin{aligned}
T^{(2)\alpha\alpha}_{ab} &= \sum_{i}^{\mathrm{occ}(\alpha)} R^{\alpha\alpha}_{ai} R^{\alpha\alpha}_{bi} + \sum_{i}^{\mathrm{occ}(\alpha)} \sum_{j}^{\mathrm{occ}(\alpha)} \Delta P^{\alpha\alpha}_{ij}(U^{\alpha\alpha}) R^{\alpha\alpha}_{ai} R^{\alpha\alpha}_{bj} \\
T^{(2)\beta\beta}_{ab} &= \sum_{a}^{\mathrm{vir}(\beta)} R^{\beta\beta}_{ai} R^{\beta\beta}_{bi}
\end{aligned}
\tag{46b}
$$

$$
\begin{aligned}
T^{(2)\alpha\alpha}_{ij} &= \sum_{a}^{\mathrm{vir}(\alpha)} R^{\alpha\alpha}_{ai} R^{\alpha\alpha}_{aj} - \sum_{l}^{\mathrm{occ}(\alpha)} \sum_{a}^{\mathrm{vir}(\alpha)} \Delta P^{\alpha\alpha}_{il}(\mathbf{U}^{\alpha\alpha}) R^{\alpha\alpha}_{al} R^{\alpha\alpha}_{aj} \\
T^{(2)\beta\beta}_{ij} &= -\sum_{i}^{\mathrm{vir}(\beta)} R^{\beta\beta}_{ai} R^{\beta\beta}_{aj}
\end{aligned}
\tag{46c}
$$

We obtain for the excitation energy

$$
\Delta E_M = \Delta E_M(U^{\alpha\alpha}) + \Delta E^R_M \tag{47}
$$

where

$$
\begin{aligned}
\Delta E_M(\mathbf{U}) = &\sum_{a}^{\mathrm{vir}(\alpha)} \varepsilon^{\alpha}_a \Delta P^{\alpha\alpha}_{aa}(\mathbf{U}^{\alpha\alpha})^2 - \sum_{i}^{\mathrm{occ}(\alpha)} - \varepsilon^{\alpha}_i \Delta P^{\alpha\alpha}_{ii}(\mathbf{U}^{\alpha\alpha})^2 \\
&+ \sum_{ab}^{\mathrm{vir}(\alpha)} \sum_{i}^{\mathrm{occ}(\alpha)} \Delta P^{\alpha\alpha}_{ai}(\mathbf{U}^{\alpha\alpha}) \Delta P^{\alpha\alpha}_{bj}(\mathbf{U}^{\alpha\alpha}) \left[K_{a_\alpha i_\alpha b_\alpha j_\alpha} + K_{a_\alpha i_\alpha b_\alpha j_\alpha} \right] \\
&+ \frac{1}{2} \sum_{ijkl}^{\mathrm{occ}(\alpha)} \Delta P^{\alpha\alpha}_{ij}(\mathbf{U}^{\alpha\alpha}) \Delta P^{\alpha\alpha}_{kl}(\mathbf{U}^{\alpha\alpha}) K_{i_\alpha j_\alpha k_\alpha l_\alpha} \\
&+ \frac{1}{2} \sum_{abcd}^{\mathrm{vir}} \Delta P^{\alpha\alpha}_{ab}(\mathbf{U}^{\alpha\alpha}) \Delta P^{\alpha\alpha}_{cd}(\mathbf{U}^{\alpha\alpha}) K_{a_\alpha b_\alpha c_\alpha d_\alpha} \\
&+ \sum_{ab}^{\mathrm{vir}(\alpha)} \sum_{ij}^{\mathrm{occ}(\alpha)} \Delta P^{\alpha\alpha}_{ab}(\mathbf{U}^{\alpha\alpha}) \Delta P^{\alpha\alpha}_{ij}(\mathbf{U}^{\alpha\alpha}) K_{a_\alpha b_\alpha i_\alpha j_\alpha} \\
&+ 2 \sum_{abc}^{\mathrm{vir}(\alpha)} \sum_{k}^{\mathrm{occ}(\alpha)} \Delta P^{\alpha\alpha}_{ab}(\mathbf{U}^{\alpha\alpha}) \Delta P^{\alpha\alpha}_{ck}(\mathbf{U}^{\alpha\alpha}) K_{a_\alpha b_\alpha c_\alpha k_\alpha} \\
&+ 2 \sum_{ijk}^{\mathrm{vir}(\alpha)} \sum_{c}^{\mathrm{occ}(\alpha)} \Delta P^{\alpha\alpha}_{ij}(\mathbf{U}^{\alpha\alpha}) \Delta P^{\alpha\alpha}_{ck}(\mathbf{U}^{\alpha\alpha}) K_{i_\alpha j_\alpha c_\alpha k_\alpha}
\end{aligned}
\tag{48}
$$

is the excitation caused by $\mathbf{U}^{\alpha\alpha}$ alone and equivalent to ΔE_M for the SCF-CV(∞)-DFT scheme of (28) but expressed in terms of canonical and unrelaxed ground state orbitals. Further

$$\Delta E_M^R = \sum_{\sigma}^{\alpha,\beta}\left(\sum_{a}^{\mathrm{vir}(\sigma)} T_{aa}^{(2)\sigma\sigma}\varepsilon_a^{\sigma} - \sum_{i}^{\mathrm{vir}(\sigma)} T_{ii}^{(2)\sigma\sigma}\varepsilon_i^{\sigma}\right) + \sum_{\sigma}^{\alpha,\beta}\sum_{\mu}^{\alpha,\beta}\sum_{a}^{\mathrm{vir}(\sigma)}\sum_{i}^{\mathrm{occ}(\sigma)}\sum_{c}^{\mathrm{vir}(\mu)} T_{ai}^{(1)\sigma\sigma}T_{bj}^{(1)\mu\mu}\left[K_{a_\sigma i_\sigma b_\mu j_\mu} + K_{a_\sigma b_\mu i_\sigma j_\mu}\right] + \sum_{\sigma}^{\alpha,\beta}\sum_{k}^{\mathrm{occ}(\sigma)}\sum_{c}^{\mathrm{vir}(\sigma)} T_{ck}^{(1)\sigma\sigma}\left[\sum_{ab}^{\mathrm{vir}(\alpha)} \Delta P_{ab}^{\alpha\alpha}(\mathbf{U}^{\alpha\alpha})K_{a_\alpha b_\alpha c_\sigma k_\sigma} + \sum_{ij}^{\mathrm{occ}(\alpha)} \Delta P_{ij}^{\alpha\alpha}(\mathbf{U}^{\alpha\alpha})K_{i_\alpha j_\alpha c_\sigma k_\sigma}\right] \tag{49}$$

is the relaxation contribution to the excitation energy. The total energy for Ψ_M is given as $E_M = E_0(\rho^0) + \Delta E_M(\mathbf{U}) + \Delta E_M^R$ where $E_0(\rho^0)$ is the ground state energy expressed in terms of unrelaxed orbitals. The expression for ΔE_M^R is derived after orthogonalization of Ψ_M to the ground state to second order in $\mathbf{R}$.

We optimize ΔE_M of (49) by first performing a Taylor expansion from the starting point reference $(\mathbf{U}^{0,\alpha\alpha}, \mathbf{R}^{0,\alpha\alpha}, \mathbf{R}^{0,\beta\beta})$ to $\left(\mathbf{U}^{\alpha\alpha}, \mathbf{R}^{\alpha\alpha}, \mathbf{R}^{\beta\beta}\right) = \left(\mathbf{U}^{0,\alpha\alpha} + \Delta\mathbf{U}^{\alpha\alpha}, \mathbf{R}^{0,\alpha\alpha} + \Delta\mathbf{R}^{\alpha\alpha}, \mathbf{R}^{0,\beta\beta} + \Delta\mathbf{R}^{\alpha\alpha}\right)$:

$$E_M\left(U^{\alpha\alpha},R^{\alpha\alpha},R^{\beta\beta}\right) = E_M\left(U^{0,\alpha\alpha},R^{0,\alpha\alpha},R^{0,\beta\beta}\right) + \sum_{ai}\left(\frac{dE_M}{dU_{ai}^{\alpha\alpha}}\right)_0 \Delta U_{ai}^{\alpha\alpha} + \sum_{\sigma}^{\alpha,\beta}\sum_{ai}\left(\frac{dE_M}{dR_{ai}^{\sigma\sigma}}\right)_0 \Delta R_{ai}^{\sigma\sigma} + \frac{1}{2}\sum_{ai}\sum_{bj}\left(\frac{d^2E_M}{dU_{ai}^{\alpha\alpha}dU_{bj}^{\alpha\alpha}}\right)_0 \Delta U_{ai}^{\alpha\alpha}\Delta U_{bj}^{\alpha\alpha} + \frac{1}{2}\sum_{ai}\sum_{bj}\sum_{\sigma}^{\alpha,\beta}\sum_{\tau}^{\alpha,\beta}\left(\frac{d^2E_M}{dR_{ai}^{\sigma\sigma}dR_{bj}^{\tau\tau}}\right)_0 \Delta R_{ai}^{\sigma\sigma}\Delta R_{bj}^{\tau\tau} + \sum_{ai}\sum_{bj}\sum_{\sigma}^{\alpha,\beta}\left(\frac{d^2E_M}{dU_{ai}^{\alpha\alpha}dR_{bj}^{\sigma\sigma}}\right)_0 \Delta U_{ai}^{\alpha\alpha}\Delta R_{bj}^{\sigma\sigma} + \mathrm{O}^{[3]} \tag{50}$$

Here the subscript "0" indicates that the derivative is evaluated at the reference $(U^{0,\alpha\alpha},R^{0,\alpha\alpha},R^{0,\beta\beta})$. We can alternatively write the expansion in terms of energy gradients and energy Hessians as

$$E_M\left(U^{\alpha\alpha},R^{\alpha\alpha},R^{\beta\beta}\right) = E_M\left(U^{0,\alpha\alpha},R^{0,\alpha\alpha},R^{0,\beta\beta}\right) + \begin{pmatrix}\Delta\vec{U}^{\alpha\alpha} & \Delta\vec{R}^{\alpha\alpha} & \Delta\vec{R}^{\beta\beta}\end{pmatrix}\begin{pmatrix}\vec{g}^{U^{\alpha\alpha}}\\ \vec{g}^{R^{\alpha\alpha}}\\ \vec{g}^{R^{\beta\beta}}\end{pmatrix} + \frac{1}{2}\begin{pmatrix}\Delta\vec{U}^{\alpha\alpha} & \Delta\vec{U}^{\alpha\alpha} & \Delta\vec{U}^{\alpha\alpha}\end{pmatrix}\begin{pmatrix}\mathbf{H}^{U^{\alpha\alpha},U^{\alpha\alpha}} & \mathbf{H}^{U^{\alpha\alpha},R^{\alpha\alpha}} & \mathbf{H}^{U^{\alpha\alpha},R^{\beta\beta}}\\ \mathbf{H}^{R^{\alpha\alpha},U^{\alpha\alpha}} & \mathbf{H}^{R^{\alpha\alpha},R^{\alpha\alpha}} & \mathbf{H}^{R^{\alpha\alpha},R^{\beta\beta}}\\ \mathbf{H}^{R^{\beta\beta},U^{\alpha\alpha}} & \mathbf{H}^{R^{\beta\beta},R^{\alpha\alpha}} & \mathbf{H}^{R^{\beta\beta},R^{\beta\beta}}\end{pmatrix}\begin{pmatrix}\mathbf{H}^{R^{\beta\beta},R^{\beta\beta}}\\ \Delta\vec{R}^{\alpha\alpha}\\ \Delta\vec{R}^{\beta\beta}\end{pmatrix} + O^{[3]} \tag{51}$$

where the expressions for the gradients $\vec{g}^{U^{\alpha\alpha}}, \vec{g}^{R^{\alpha\alpha}}, \vec{g}^{R^{\beta\beta}}$ and Hessians $\mathbf{H}^{U^{\alpha\alpha},U^{\alpha\alpha}}$, $H^{R^{\alpha\alpha},U^{\alpha\alpha}}$, etc. can be obtained by a comparison between (50) and (51). Specific

formula for $\vec{g}^{U^{\alpha\alpha}}$, $\vec{g}^{R^{\alpha\alpha}}$, and $\vec{g}^{R^{\beta\beta}}$ are also given in [26] for the spin-flip transition.

For the spin conserving transition, a differentiation of (51) with respect to the individual components of $\Delta\vec{U}^{\alpha\alpha}$, $\Delta\vec{R}^{\alpha\alpha}$, and $\Delta\vec{R}^{\beta\beta}$ affords, after rearrangement,

$$\begin{pmatrix} \vec{g}^{U^{\alpha\alpha}}(0) \\ \vec{g}^{R^{\alpha\alpha}}(0) \\ \vec{g}^{R^{\beta\beta}}(0) \end{pmatrix} + \begin{pmatrix} \mathbf{H}^{U^{\alpha\alpha},U^{\alpha\alpha}}(0) & \mathbf{H}^{U^{\alpha\alpha},R^{\alpha\alpha}}(0) & \mathbf{H}^{U^{\alpha\alpha},R^{\beta\beta}}(0) \\ \mathbf{H}^{R^{\alpha\alpha},U^{\alpha\alpha}}(0) & \mathbf{H}^{R^{\alpha\alpha},R^{\alpha\alpha}}(0) & \mathbf{H}^{R^{\alpha\alpha},R^{\beta\beta}}(0) \\ \mathbf{H}^{R^{\beta\beta},U^{\alpha\alpha}}(0) & \mathbf{H}^{R^{\beta\beta},R^{\alpha\alpha}}(0) & \mathbf{H}^{R^{\beta\beta},R^{\beta\beta}}(0) \end{pmatrix} \begin{pmatrix} \Delta\vec{U}^{\alpha\alpha} \\ \Delta\vec{R}^{\alpha\alpha} \\ \Delta\vec{R}^{\beta\beta} \end{pmatrix} = 0 \quad (52)$$

from which we can find $\left(\Delta\vec{U}^{\alpha\alpha}, \Delta\vec{R}^{\alpha\alpha}, \Delta\vec{R}^{\beta\beta}\right)$ iteratively. More details can be found in [26] which also covers the case of spin-flip transitions.

2.5.1 Application of RSCF-CV(∞)-DFT to $n_\sigma \rightarrow \pi^*$ Transitions

It follows from Table 4 that the RSCF-CV(∞)-DFT scheme with full orbital relaxation gives $n_\sigma \rightarrow \pi^*$ transition energies which on average are within 0.15 eV of the ΔSCF results. This is acceptable given the fact that the RSCF-CV(∞)-DFT scheme is only second order in relaxation and that it satisfies constraints not fulfilled by ΔSCF. In comparison to the "Best" ab initio results [73], RSCF-CV (∞)-DFT fares as well as ΔSCF and CV(2)-TD (TDDFT-TD) with an RMSD of 0.32 eV. Thus, although RSCF-CV(∞)-DFT is somewhat more costly (~twice) for each transition, it does not fare much better than CV(2)-TD in those cases where the latter is reliable and fares well. However, what we show shortly is that RSCF-CV (∞)-DFT has a similar accuracy (RMSD ~0.3–0.2 eV) where CV(2)-TD fails such as Rydberg and charge transfer transitions.

2.5.2 Application of RSCF-CV(∞)-DFT to Rydberg Transitions

We have benchmarked [66] the performance of RSCF-CV-DFT in studies on Rydberg transitions employing five different standard functionals and a diffuse basis; see Table 5. Our survey is based on 71 triplet or singlet Rydberg transitions distributed over 9 different species: N_2(5), CO (7), CH_2O (8), C_2H_2 (8), H_2O (10), C_2H_4 (13), Be (6), Mg (6), and Zn (8). The best performance comes from the long range corrected functional LCBP86 ($\omega = 0.4$.) with an average root mean square deviation (RMSD) of 0.23 eV. Of similar accuracy are LDA and B3LYP, both with an RMSD of 0.24 eV. The largest RMSD of 0.32 eV come from BP86 and LCBP86* ($\omega = 0.75$). The performance of RSCF-CV-DFT is considerably better than that of adiabatic time-dependent density functional theory (ATDDFT) and matches that of highly optimized long range corrected functionals. However, it is not as accurate as ATDDFT based on highly specialized functionals.

Table 5 Root mean square deviations of Rydberg excitation energies[a] calculated with RSCF-CV (∞)-DFT using five functionals with the extended basis set [66]

Species	Nr. of States	Functionals				
		LDA	BP86	B3LYP	LCBP86[b]	LCBP86*[c]
N_2	5	0.27	0.34	0.05	0.23	0.62
CO	7	0.22	0.43	0.13	0.12	0.37
CH_2O	8	0.21	0.28	0.12	0.20	0.34
C_2H_2	8	0.31	0.50	0.52	0.25	0.24
H_2O	10	0.27	0.17	0.14	0.21	0.24
C_2H_4	13	0.15	0.20	0.28[d]	0.28	0.29
Be	6	0.45	0.60	0.47	0.31	0.23
Mg	6	0.18	0.35	0.19	0.13	0.12
Zn	8	0.18	0.25	0.27	0.34	0.46
Average root mean square deviation		0.24	0.32	0.24	0.23	0.32

[a]Energies in eV
[b]Refers to LC functional combined with BP86 and $\omega = 0.4$
[c]Represents LC functional combined with BP86 and $\omega = 0.75$
[d]Comprised of 12 states

The reasonable success of RSCF-CV-DFT is based on its well documented ability to afford good estimates of ionization potentials (IP) and electron affinities (EA) even for simple local functionals after orbital relaxation has been taken into account [66]. In adiabatic time-dependent density functional theory (ATDDFT) based on regular functionals, both IP and -EA are poorly described with errors of up to 5 eV [66]. In the transition energy ($\Delta E = \text{IP} - \text{EA}$) these errors are cancelled to some degree. However, ΔE still carries an error exceeding 1 eV [66].

2.5.3 Application of RSCF-CV(∞)-DFT to Charge Transfer Transitions

It has been demonstrated that regular adiabatic TDDFT employing the general gradient approximation (GGA) as well as hybrid functionals with a fraction (α) of exact Hartree–Fock exchange included $(0.0 \leq \alpha \leq 0.5)$ underestimate charge transfer excitation energies by as much as 2–4 eV [24, 25, 33]. This failure has been discussed and analyzed extensively [24, 25, 32, 33]. By contrast, ATDDFT in conjunction with long range corrected (LC) functionals affords charge transfer excitation energies in good agreement with experiment [33]. In these functionals, Hartree–Fock exchange is given a growing weight towards longer inter-electronic distances.

We have recently [30] applied the RSCF-CV(∞)-DFT scheme to a series of charge transfer molecular complexes (CTMC) of the type X-TCNE where an aromatic molecule (X = benzene, toluene, *o*-xylene, naphthalene, anthracene) is bound to tetracyanoethylene (TCNE) [33]. All of these complexes have one or more distinct charge transfer transitions involving the excitation of an electron from an

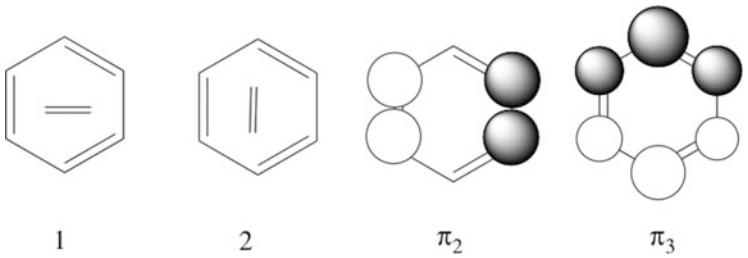

Fig. 6 Conformations and frontier orbitals in the benzene-TCNE adduct

occupied π-orbital on X to the empty π-orbital on TCNE. The X-TCNE complexes were first introduced by Stein et al. [33] as a benchmark set for CT-transitions in connection with their study on the performance of LC functionals.

The charge transfer spectrum for the series of adducts X-TCNE (X=benzene, toluene, *o*-xylene, and naphthalene, TCNE=tetracyanoethylene) has been studied extensively by experimental [84–88] and computational techniques [32, 89]. The experimental investigations include both gas phase [88] and solvation studies [85, 86] whereas the computational examinations have made use of high level ab initio schemes [89] and methods based on density functional theory [24, 25, 32, 33].

The simple adduct between benzene and TCNE has in the ground state two conformational minima of C_{2V} symmetry given as **1** and **2** in Fig. 6. The minima are calculated in both gas phase and solution to be separated by at most 0.7 kcal. Each conformation gives rise to one allowed and one forbidden transition. These transitions are to the same π^* LUMO orbital of TCNE but originate from two different HOMO orbitals on benzene; see π_2 and π_3 of Fig. 6. The four calculated transitions from π_2 and π_3 in **1** and **2** differ by less than 0.05 eV.

It is thus not surprising that the experimental spectrum in both gas phase and solution exhibits one (broad) CT-band at room temperature. The CT spectrum in gas phase has a halfwidth of 0.8 eV and a maximum at 3.59 eV [88]. This maximum is in a dichloromethane solution shifted to 3.25 eV. We exhibit in Table 6 [30] the calculated CT-excitation energies for CV(2)-DFT, CV(∞)-DFT, SCF-CV(∞)-DFT, and RSCF-CV(∞)-DFT using LDA, BP86, B3LYP, BHLYP, LCBP86, and HF.

We note in Table 6 for CV(2)-TD (ATDDFT-TD) that local functionals underestimate the experimental charge transfer excitation energy (3.59 eV [88]). The calculated excitation energies are still too low for the hybrids B3LYP and BHLYP, whereas the long range corrected functional LC-BP86 is now within 0.1 eV of experiment. For the perturbative P-CV(∞) approach, calculated ΔE_S values in Table 6 are in general seen to be higher than the observed excitation energy by more than 1 eV. This is understandable because the "excited state" determinants in P-CV(∞) are constructed from U vectors optimized with respect to CV(2)-TD. Further, all relaxation is neglected. In the SCF-CV(∞)-DFT scheme the excited state energy is minimized with respect to U while relaxation is still neglected. This leads to some improvement. However, the best results are obtained with RSCF-CV

Table 6 Calculated excitation energies[a] for benzene-TCNE[f]

	CV(2)-TD[b]	P-CV(∞)[c]	SCF-CV (∞)[d]	RSCF-CV (∞)[e]
LDA	1.40	4.99	3.64	3.30
BP86	1.37	4.92	3.69	3.32
B3LYP	1.85	4.89	4.38	3.56
BHLYP	2.75	4.80	4.76	3.31
LC-BP86	3.74	4.92	4.69	3.10
HF	4.70	4.72	4.53	2.85

[a]Energies in eV
[b]Second order energies identical to adiabatic TD-DFT within the Tamm–Dancoff approximation
[c]Energies to all orders in U. Matrix U taken from CV(2)
[d]Energies to all orders in U. Matrix U optimized with respect to the SCF-CV(∞) energy expression
[e]SCF-CV(∞) with orbital relaxation
[f]Allowed transition in conformation **2** involving the transition from π_2 of benzene to π^* of TCNE

Table 7 RSCF-CV(∞) calculations on the TCNE adducts I–IV from [30]

Functional	I	II	III	IV
LDA	3.30	2.91	2.70	2.40
BP86	3.32	2.93	2.73	2.42
B3LYP	3.56	3.19	3.05	2.44
BHLYP	3.31	3.10	2.84	2.40
LC-BP86	3.10	2.90	2.60	2.29
Exp	3.56	3.32	3.15	2.60

(∞)-DFT where the energy is minimized with respect to both R and U. After full optimization in RSCF-CV(∞)-DFT, the calculated excitation energies are lowered from CV(∞)-TD to values in reasonable agreement with experiment. The best fit is provided by B3LYP (3.56 eV) and the largest deviation is observed for LC-BP86 (3.10 eV). We must conclude that the RSCF-CV(∞)-DFT method in general gives reasonably good agreement with experiment for the different DFT schemes. Thus the RSCF-CV(∞)-DFT energy expressions of (28) and (29) seem to be relatively robust with respect to the choice of functional; see Table 6. The relaxation brings the calculated excitation energy to 2.85 eV for RSCF-CV(∞)-HF; see Table 6 [30].

We present in Table 7 [30] RSCF-CV(∞) results for calculations on X-TCNE adducts I-IV of Fig. 7 using both local functionals and hybrids together with long range corrected (LC) functionals. We notice again that the standard functionals LDA, BP86, B3LYP, and BHLYP all are close to experiment. The LC-BP86 functional fares somewhat worse here. However, we have not optimized the LC parameter which usually improves the results [33]. It should be noted that the corresponding ATDDFT results are off by 2 eV for LDA, BP86, 1 eV for B3LYP and BHLYP [30, 33]. For optimized LC functionals the ATDDFT results are in excellent agreement with experiment [33].

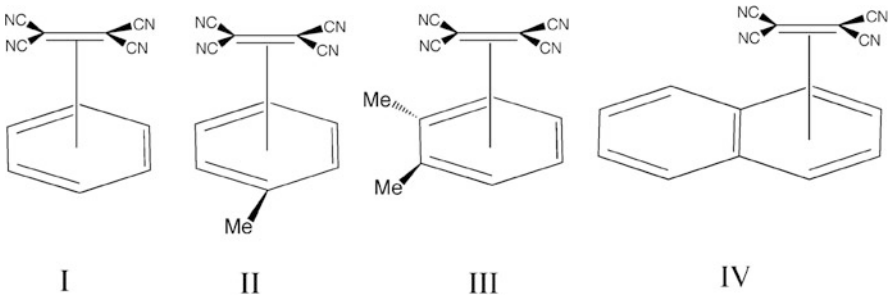

Fig. 7 Adducts I–IV of Table 7

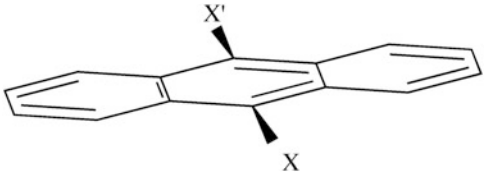

Fig. 8 Different anthracene complexes examined by the RP-CV(4)-DFT scheme

Table 8 Singlet excitation energies (in eV) for π (donor) to π^* (TCNE) transitions in X-anthracene complexes based on a TZP-basis and the RP-CV(4) scheme with different functionals

Substituents(X)	LDA	BP86	BLYP	BPErev	SAOP	GRAC	SKB	Exp.
None	1.69	1.71	1.66	1.73	1.60	1.71	1.82	1.73
9,10-Dimethyl	1.43	1.46	1.41	1.47	1.34	1.45	1.77	1.44
9-Carbo-methoxy	1.74	1.78	1.70	1.80	1.71	1.77	1.84	1.84
9-Chloro	1.74	1.78	1.71	1.80	1.66	1.78	1.82	1.74
9-Cyano	2.00	2.03	1.96	2.04	1.97	2.00	2.03	2.01
9-Formyl 10-chloro	2.02	2.06	1.99	2.08	1.80	2.06	1.96	1.96
9-Formyl	1.99	2.03	1.97	2.05	1.97	2.04	1.95	1.90
9-Methyl	1.48	1.50	1.45	1.51	1.44	1.49	1.71	1.55
9-Nitro	1.94	1.97	1.92	1.99	1.96	1.98	2.12	2.03
RMSD	0.06	0.07	0.08	0.07	0.10	0.07	0.10	1.73

VWN [90], BP86 [91, 92], BLYP [91, 93], revPBE [94–96], SAOP [97], SKB [33], GRAC [98]

In a method which predates RSCF-CV(∞) we combined P-CV(n) with orbital relaxation (RP-CV(n)) to study charge transfer transitions in a series of substituted anthracene–TCNE systems with various groups in the meso position where $n = 4$ [31]. Our results for the series X-anthracene of Fig. 8 are given in Table 8. Experimentally, X-anthracene with pure anthracene or alkyl substituted anthracenes have smaller excitation energies than X-anthracene systems with polar oxygen or a CN group. This order is more or less reproduced by R-CV(4)-DFT. The functional dependence shown in Table 8 is minor. Excitation energies

calculated by the GGA functionals BP86, BLYP, and revBEP differ on average by less than 0.05 eV from LDA estimates and introducing SAOP or GRAC with the right asymptotic 1/r behavior does not lead to any significant change. Charge transfer transitions can also be described well by the variational DFT-based spin-restricted ensemble referenced Kohn–Sham (REKS) method [57] (see footnote 1).

It is at this point important to note that the experimental excitation energies for the anthracene systems were all obtained in solution with CH_3Cl as the solvent. We do not expect the solvent effect to be significant. In fact, theoretical calculations [33] using a continuum model revealed that the excitation energies were lower by only 0.05 eV. We have, as a consequence, decided to compare our gas-phase results directly with the experimental solvent data. We obtain from such a comparison that the RMSD is 0.06 for LDA followed by 0.07 for BP86, revPBE, and 0.08 for BLYP. The two 1/r asymptotically corrected functionals afford 0.10 for SAOP and 0.07 for CRAC. Stein et al. [33] "SKB" introduced in their DZP gas-phase study a uniform correction of -0.32 eV to simulate solvation effects; see Table 8. The magnitude and sign of this correction was given without much explanation [33]. After applying their correction the authors obtained an RMSD of 0.1 which is quite similar to the one found here for our gas-phase results without any solvent correction. It should be noted that ATDDFT with the same functionals carries errors of up to 1 eV.

3 Concluding Remarks

We have here reviewed the theoretical foundation of constricted variational density functional theory and illustrated its scope through applications. CV(n)-DFT encompasses adiabatic TDDFT and ΔSCF-DFT as special cases. Thus our variational second order CV(2)-DFT is identical to adiabatic TDDFT ground state response theory [29, 62] and ΔSCF-DFT is the same as RSCF-CV(∞)-DFT in the case where the transition is described by a single orbital replacement with γ of (18) equal to $\pi/2$ [28]. CV(n)-DFT can be used as a natural extension of adiabatic TDDFT. The first step in this direction is the perturbative P-CV(∞)-DFT approach [64] in which the **U** from CV(2)-DFT is used to calculate the all order energy in CV(∞)-DFT [27, 64]. It is shown to work well for $\pi \rightarrow \pi^*$ transitions in conjugated systems. At a higher level, **U** is optimized with respect to the all order energy in CV(∞)-DFT scheme leading to SCF-CV(∞)-DFT [28]. Experience has shown [27, 63] that optimization of **U** alone is insufficient. One also has to relax all the other occupied orbitals which do not directly participate in the transition. This is done in SCF-CV (∞)-DFT by introducing orbital relaxation (RSCF-CV(∞)-DFT) [26]. The RSCF-CV(∞)-DFT scheme differs from adiabatic TDDFT (CV(2)-DFT) by going to all orders in **U** and by introducing orbital relaxation. The extra effort involved in connection with RSCF-CV(∞)-DFT compared to adiabatic TDDFT does not result in improved accuracy for cases where adiabatic TDDFT fares well, such as for the $\pi \rightarrow \pi^*$ transition [26]. However, it does not fail for charge transfer [30, 31] and Rydberg transitions [66] in the way adiabatic TDDFT does for regular functionals.

This is an important point in studies of absorption spectra where many different types of transitions are present.

In CV-DFT we use approximate ground state functionals in a variational description of the excited states. Such a procedure is consistent with AD-TDDFT in that this theory is equivalent to CV(2)-DFT within the TD-approximation. Going beyond the adiabatic approximation by introducing frequency-dependent kernels consistent with the approximate ground state functional in TDDFT has proven difficult. Here we go beyond CV(2)-DFT in a variational approach, still using an approximate ground state functional but introducing an optimization of U based on the KS-energy to all orders in $\mathbf{U}$ as well as relaxation of the inactive orbitals. It is hoped that going beyond CV(2) in this way is equivalent to introducing a frequency-dependent kernel in TDDFT. Obviously with such a kernel, inactive orbitals would be different from those of the ground state and vary between excited states as in the RSCF-CV(∞) scheme. Further, with a frequency-dependent kernel and related Hessian, the $\mathbf{U}$ matrix obtained for each excited state should be different from that determined by the ground state Hessian in AD-TDDFT, just as in the SCF-CV(∞)-DFT scheme. At present, CV-DFT has the same problems as TDDFT with regards to bond dissociation. Work is under way to introduce doubles into the description of one-electron transitions [99, 100]. This should ensure a prober bond dissociation and provides for a better description of the electron spectra of polyenes [36]. The perturbative P-CV(∞)-DFT approach doubles the time required for each excitation compared to TDDFT, whereas the increase is fivefold for RSCF-CV(∞). This might change with more efficient iterative procedures.

Acknowledgement T.Z. would like to thank the Canadian government for a Canada research chair in theoretical inorganic chemistry and NSERC for financial support.

References

1. Jensen F (2006) Introduction to computational chemistry. Wiley, New York
2. Helgaker T, Jørgensen P, Olsen J (2000) Molecular electronic-structure theory. Wiley, New York
3. Runge E, Gross EKU (1984) Density functional theory for time-dependent systems. Phys Rev Lett 52:997
4. Casida ME (1995) In: Chong DP (ed) Recent advances in density functional methods. World Scientific, Singapore, pp 155–193
5. van Gisbergen SJA, Snijders JG (1995) A density functional theory study of frequency dependent polarizabilities and Van der Waals dispersion coefficients for polyatomic molecules. J Chem Phys 103:9347
6. Petersilka M, Grossmann UJ, Gross EKU (1996) Excitation energies from time-dependent density-functional theory. Phys Rev Lett 76:12
7. Bauernschmitt R, Ahlrichs R (1996) Treatment of electronic excitations within the adiabatic approximation of time dependent density functional theory. Chem Phys Lett 256:454
8. Furche F (2001) On the density matrix based approach to time-dependent density functional response theory. J Chem Phys 114:5882

9. Furche F, Ahlrichs R (2002) Adiabatic time-dependent density functional methods for excited state properties. J Chem Phys 117:7433
10. Romaniello P, Sangalli D, Berger JA, Sottile F, Molinari LG, Reining L, Onida G (2009) Double excitations in finite systems. J Chem Phys 130:044108
11. Gritsenko O, Baerends EJ (2009) Double excitation effects in non-adiabatic time-dependent theory with an analytic construction of the exchange correlation kernel in the common energy denominator energy approximation. Phys Chem 11:4640
12. Jacquemin D, Wathelet V, Perpète EA, Adamo C (2009) Extensive TD-DFT benchmark: singlet excited states of organic molecules. J Chem Theory Comput 5:2420
13. Jacquemin D, Perpète EA, Ciofini I, Adamo C (2009) Accurate simulation of optical properties in dyes. Acc Chem Res 42:326
14. Jacquemin D, Perpete EA, Scuseria GE, Ciofini I, Adamo C (2008) TD-DFT performance for the visible absorption spectra of organic dyes: conventional versus long range hybrids. J Chem Theory Comput 4:123–135
15. Grimme S, Neese F (2007) Double-hybrid density functional theory for excited electronic states of molecules. J Chem Phys 127:154116
16. Send R, Valsson O, Filippi C (2011) Electronic excitations of simple cyanine dyes: reconciling density functional and wave function methods. J Chem Theory Comput 7:444
17. Jacquemin D, Perpete EA, Ciofini I, Adamo C, Valero R, Zhao Y, Truhlar DG (2010) On the performances of the M06 family of density functionals for electronic excitation energies. J Chem Theory Comput 6:2071
18. Moore B II, Autschbach J (2013) Longest-wavelength electronic excitations of linear cyanines: the role of electron delocalization and of approximations in time-dependent density functional theory. J Chem Theory Comput 9:4991
19. Schipper PRT, Gritsenko OV, van Gisberger SJA, Baerends EJ (2000) Molecular calculations of excitation energies and (hyper)polarizabilities with a statistical average of orbital model exchange-correlation potentials. J Chem Phys 112:1344
20. Likura H, Tsuneda T, Tanai T, Hirao K (2001) A long-range correction scheme for generalized-gradient-approximation exchange functionals. J Chem Phys 115:3540
21. Song J-W, Watson MA, Hirao K (2009) An improved long-range corrected hybrid functional with vanishing Hartree–Fock exchange at zero interelectronic distance (LC2gau-BOP). J Chem Phys 131:144108
22. Heyd J, Scuseria GE, Ernzerhof M (2003) Hybrid functionals based on a screened Coulomb potential. J Chem Phys 118:8207
23. Baer R, Neuhauser D (2005) Density functional theory with correct long-range asymptotic behavior. Phys Rev Lett 94:043002
24. Dreuw A, Weisman J, Head-Gordon M (2003) Long-range charge-transfer excited states in time-dependent density functional theory require non-local exchange. J Chem Phys 119:2943
25. Tozer D (2003) Relationship between long-range charge transfer error and integer discontinuity error in Kohn Sham theory. J Chem Phys 119:12697
26. Krykunov M, Ziegler T (2013) Self-consistent formulation of constricted variational density functional theory with orbital relaxation. Implementation and application. J Chem Theory Comput 9:2761
27. Ziegler T, Krykunov M, Cullen J (2012) The implementation of a self-consistent constricted variational density functional theory for the description of excited states. J Chem Phys 136:124107
28. Cullen J, Krykunov M, Ziegler T (2011) The formulation of a self-consistent constricted variational density functional theory for the description of excited states. Chem Phys 391:11
29. Ziegler T, Seth M, Krykunov M, Autschbach J, Wang F (2009) On the relation between time-dependent and variational density functional theory approaches for the determination of excitation energies and transition moments. J Chem Phys 130:154102
30. Krykunov M, Seth M, Ziegler T (2014) Derivation of the RPA (random phase approximation) equation of ATDDFT (adiabatic time dependent density functional ground state response

theory) from an excited state variational approach based on the ground state functional. J Chem Phys 140:18A502
31. Ziegler T, Krykunov M (2010) On the calculation of charge transfer transitions with standard density functionals using constrained variational density functional theory. J Chem Phys 133:074104
32. Ziegler T, Seth M, Krykunov M, Autschbach J, Wang F (2008) A revised electronic Hessian for approximate time-dependent density functional theory. J Chem Phys 129:184114
33. Stein T, Kronik L, Baer R (2009) Reliable prediction of charge transfer excitations in molecular complexes using time-dependent density functional theory. J Am Chem Soc 131:2818
34. Cave RJ, Zhang F, Maitra NT, Burke K (2004) A dressed time-dependent density functional treatment of the 2^1A states of butadiene and hexatriene. Chem Phys Lett 389:39
35. Mazur G, Wlodarczyk R (2009) Application of the dressed time-dependent density functional theory for the excited states of linear polyenes. J Comp Chem 30:811
36. Elliott P, Goldson S, Canahui C, Maitra NT (2011) Perspectives on double-excitations in TDDFT. Chem Phys 391:110
37. Slater JC, Wood JH (1971) Statistical exchange and the total energy of a crystal. Int J Quant Chem Suppl 4:3
38. Slater JC (1972) Statistical exchange-correlation in the self-consistent field. Adv Quant Chem 6:1
39. Kowalczyk T, Yost SR, Van Voorhis T (2011) Assessment of the ΔSCF density functional theory approach for electronic excitations in organic dyes. J Chem Phys 134:054128
40. Ziegler T, Rauk R, Baerends EJ (1977) On the calculation of multiplet energies by the Hartree-Fock-Slater method. Theor Chim Acta 43:261
41. Ziegler T, Rauk A, Baerends EJ (1976) The electronic structure of tetrahedral oxo-complexes. The nature of the "charge transfer" transitions. J Chem Phys 16:209
42. Gilbert A, Besley N, Gill P (2008) J Phys Chem A 122:13164
43. Besley N, Gilbert A, Gill P (2009) Self-consistent-field calculations of core excited states. J Chem Phys 130:124308-1
44. Park YC, Krykunov M, Seidu I, Ziegler T (2014) On the relation between adiabatic time dependent density functional theory (TDDFT) and the ΔSCF-DFT method. Introducing a numerically stable ΔSCF-DFT scheme for local functionals based on constricted variational DFT. Mol Phys 112:661
45. Gavnholt J, Olsen T, Engelund M, Schiøtz J (2008) Δ self-consistent field method to obtain potential energy surfaces of excited molecules on surfaces. J Phys Rev B 78:075441/1
46. Liu TQ, Han WG, Himo FG, Ullmann M, Bashford D, Toutchkine A, Hahn KM, Noodleman L (2004) Density functional vertical self-consistent reaction field theory for solvatochromism studies of solvent-sensitive dyes. Phys Chem A 108:3545
47. Ceresoli D, Tosatti E, Scandolo S, Santoro G, Serra S (2004) Trapping of excitons at chemical defects in polyethylene. J Chem Phys 121:6478
48. Zhekova H, Seth M, Ziegler T (2014) Application of time dependent and time independent density functional theory to the first π to π* transition in cyanine dyes. Int J Quant Chem 114:1019
49. Ziegler T (2011) A chronical about the development of electronic structure theories for transition metal complexes. Struct Bond 47:1
50. von Barth U (1979) Local-density theory of multiplet structure. Phys Rev A 20:1693
51. Gunnarsson O, Lundqvist BI (1976) Exchange and correlation in atoms, molecules, and solids by the spin-density-functional formalism. Phys Rev B 13:4274
52. Levy M, Perdew JP (1985) Hellmann-Feynman, virial, and scaling requisites for the exact universal density functionals. Shape of the correlation potential and diamagnetic susceptibility for atoms. Phys Rev A 32:2010
53. Gaudoin R, Burke K (2005) Lack of Hohenberg-Kohn theorem for excited states. Phys Rev Lett 93:173001

54. Oliveira LN, Gross EKU, Kohn W (1988) Density-functional theory for ensembles of fractionally occupied states. II. Application to the He atom. Phys Rev A 37:2821
55. Filatov M, Shaik S (1998) Spin-restricted density functional approach to the open-shell problem. Chem Phys Lett 288:689
56. Filatov M, Shaik S (1999) Spin-restricted density functional approach to the open-shell problem. Chem Phys Lett 304:429
57. Filatov M, Huix-Rotllant M (2014) Description of electron transfer in the ground and excited states of organic donor–acceptor systems by single-reference and multi-reference density functional methods. J Chem Phys 141:024112
58. Gidopoulos NI, Papaconstantinou PG, Gross EKU (2002) Density-functional theory for ensembles of fractionally occupied states. II. Application to the He atom. Phys Rev Lett 88:03300
59. Gross EKU, Oliveira LN, Kohn W (1988) Spurious interactions, and their correction, in the ensemble-Kohn-Sham scheme for excited states. Phys Rev A 37:2809
60. Levy M, Nagy A (1999) Variational density-functional theory for an individual excited state. Phys Rev Lett 83:4361
61. Görling A, Levy M (1993) Correlation-energy functional and its high-density limit obtained from a coupling-constant perturbation expansion. Phys Rev B 47:13105
62. Ziegler T, Krykunov M, Autschbach J (2014) Derivation of the RPA (random phase approximation) equation of ATDDFT (adiabatic time dependent density functional ground state response theory) from an excited state variational approach based on the ground state functional. J Chem Theory Comput 10:3980
63. Ziegler T, Krykunov M, Cullen J (2011) The application of constricted variational density functional theory to excitations involving electron transitions from occupied lone-pair orbitals to virtual π* orbitals. J Chem Theory Comput 7:2485
64. Krykunov M, Grimme S, Ziegler T (2012) Accurate theoretical description of the ^1L_a and ^1L_b excited states in acenes using the all order constricted variational density functional theory method and the local density approximation. J Chem Theory Comput 8:4434
65. Zhekova H, Krykunov M, Autschbach J, Ziegler T (2014) Applications of time dependent and time independent density functional theory to the first π to π* transition in cyanine dyes. J Chem Theory Comput 10:3299
66. Seidu I, Krykunov M, Ziegler T (2014) Applications of time--dependent and time-- independent density functional theory to Rydberg transitions. J Phys Chem A ASAP. doi:10.1021/jp5082802
67. Wang F, Ziegler T (2004) Time-dependent density functional theory based on a noncollinear formulation of the exchange-correlation potential. J Chem Phys 121:12191-1
68. Wang F, Ziegler T (2005) The performance of time-dependent density functional theory based on a noncollinear exchange-correlation potential in the calculations of excitation energies. J Chem Phys 122:074109-1
69. Wang F, Ziegler T (2006) Use of noncollinear exchange-correlation potentials in multiplet resolutions by time-dependent density functional theory. Int J Quant Chem 106:2545–2550
70. Hirata S, Head-Gordon M (1999) Time-dependent density functional theory within the Tamm-Dancoff approximation. Chem Phys Lett 291:314
71. Amos AT, Hall GG (1961) Single determinant wave functions. Proc R Soc A 263:483
72. Martin RLJ (2003) Natural transition orbitals. J Chem Phys 118:4775
73. Schreiber M, Silva-Junior M, Sauer S, Thiel W (2008) Benchmarks for electronically excited states: CASPT2, CC2, CCSD, and CC3. J Chem Phys 128:134110
74. Platt JR (1949) Classification of spectra of Cata condensed hydrocarbons. J Chem Phys 17:484
75. Grimme S, Parac M (2003) Substantial errors from time-dependent density functional theory for the calculation of excited states of large π systems. Chemphyschem 4:292
76. Parac M, Grimme S (2003) TDDFT of the lowest excitation energies of polycyclic aromatic hydrocarbons. Chem Phys 292:11

77. Jacquemin D, Wathelet V, Perpete EA, Adamo C (2009) Assessment of functionals for TD-DFT calculations of singlet-triplet calculations. J Chem Theory 5:2420
78. Goerigk L, Grimme S (2010) Assessment of TD-DFT methods and of various spin scaled CIS (D) and CC2 versions for the treatment of low-lying valence excitations of large organic dyes. J Chem Phys 132:184103
79. Richard RM, Herbert JM (2011) Time-dependent density-functional description of the 1La state in polycyclic aromatic hydrocarbons: charge-transfer character in disguise? J Chem Theory Comput 7:1296
80. Ziegler T, Rauk A (1977) On the calculation of bonding energies by the Hartree-Fock-Slater method. Theor Chim Acta (Berl) 46:1
81. Pople JA, Krishnan R, Schlegel HB, Binkley JS (1979) Derivative studies in configuration interaction theory. Int J Quant Chem S13:225
82. Fletcher R (1980) Practical methods of optimization, vol 1. Wiley, New York
83. Fischer H, Almlöf J (1992) General methods for geometry and wave function optimization. J Phys Chem 96:9768
84. Prochorow J, Tramer AJ (1967) Photoselection study of charge transfer complexes. J Chem Phys 47:775
85. Frey JE, Andrews AM, Ankoviac DG et al (1990) Charge-transfer complexes of tetracyanoethylene with cycloalkanes, alkenes, and alkynes and some of their aryl derivatives. J Org Chem 55:606
86. Merrifield RE, Phillips WD (1958) Cyanocarbon chemistry. II.1 Spectroscopic studies of the molecular complexes of tetracyanoethylene. J Am Chem Soc 80:2778
87. Masnovi JM, Seddon EA, Kochi JK (1984) Electron transfer from anthracenes. Comparison of photoionization, charge-transfer excitation and electrochemical oxidation. Can J Chem 62:2552
88. Hanazaki I (1972) Vapor-phase electron donor–acceptor complexes of tetracyanoethylene and of sulfur dioxide. J Phys Chem 76:1982
89. Garcia-Cuesta I, Sanchez de Meras AMJ, Koch H (2003) Coupled cluster calculations of the vertical excitation energies of tetracyanoethylene. J Chem Phys 118:8216
90. Vosko SH, Wilk L, Nusair M (1980) Accurate spin-dependent electron liquid correlation energies for local spin density calculations: a critical analysis. Can J Phys 58:1200
91. Becke AD (1988) Density-functional exchange-energy approximation with correct asymptotic behavior. Phys Rev A 38:3098
92. Perdew JP, Wang Y (1986) Density-functional approximation for the correlation energy of the inhomogeneous electron gas. Phys Rev B 33:8822
93. Lee C, Yang W, Parr RG (1988) Development of the Colle-Salvetti correlation-energy formula into a functional of the electron density. Phys Rev B 37:785
94. Perdew JP, Burke K, Ernzerhof M (1996) Generalized gradient approximation made simple. Phys Rev Lett 77:3865
95. Hammer B, Hansen LB, Norskøv JK (1999) Improved adsorption energetics within density-functional theory using revised Perdew-Burke-Ernzerhof functionals. Phys Rev B 59:7413
96. Zhang Y, Yang W (1998) Comment on "generalized gradient approximation made simple". Phys Rev Lett 80:890
97. Gritsenko OV, Schipper PRT, Baerends EJ (1999) Approximation of the exchange-correlation Kohn–Sham potential with a statistical average of different orbital model potentials. Chem Phys Lett 302:199
98. Grüning M, Gritsenko OV, van Gisbergen SJA, Baerends EJ (2001) Shape corrections to exchange-correlation Kohn-Sham potentials by gradient-regulated seamless connection of model potentials for inner and outer region. J Chem Phys 114:652
99. Filatov M (2013) Assessment of density functional methods for obtaining geometries at conical intersections in organic molecules. J Chem Theory Comput 9:4526
100. Ziegler T (1983) Extension of the statistical energy expression to multi-determinantal wave functions. In: Dahl JP, Avery J (eds) Density functional theory of atoms, molecules and solids. Plenum, New York